Chapter 9
Outskirts of Distant Galaxies in Absorption

Hsiao-Wen Chen

Abstract QSO absorption spectroscopy provides a sensitive probe of both the neutral medium and diffuse ionized gas in the distant Universe. It extends 21 cm maps of gaseous structures around low-redshift galaxies both to lower gas column densities and to higher redshifts. Combining galaxy surveys with absorption-line observations of gas around galaxies enables comprehensive studies of baryon cycles in galaxy outskirts over cosmic time. This chapter presents a review of the empirical understanding of the cosmic neutral gas reservoir from studies of damped Lyα absorbers (DLAs). It describes the constraints on the star formation relation and chemical enrichment history in the outskirts of distant galaxies from DLA studies. A brief discussion of available constraints on the ionized circumgalactic gas from studies of lower column density Lyα absorbers and associated ionic absorption transitions is presented at the end.

9.1 Introduction

Absorption-line spectroscopy complements emission surveys and provides a powerful tool for studying the diffuse, large-scale baryonic structures in the distant Universe (e.g. Rauch 1998; Wolfe et al. 2005; Prochaska and Tumlinson 2009). Depending on the physical conditions of the gas (including gas density, temperature, ionization state and metallicity), a high-density region in the foreground is expected to imprint various absorption transitions of different line strengths in the spectrum of a background QSO. Observing the absorption features imprinted in QSO spectra enables a uniform survey of diffuse gas in and around galaxies, as well as detailed studies of the physical conditions of the gas at redshifts as high as the background sources can be observed.

Figure 9.1 displays an example of optical and near-infrared spectra of a high-redshift QSO. The QSO is at redshift $z_{QSO} = 4.13$, and the spectra are retrieved from the XQ-100 archive (Lopez et al. 2016). At the QSO redshift, multiple broad

H.-W. Chen (✉)

Department of Astronomy & Astrophysics, and Kavli Institute for Cosmological Physics,
The University of Chicago, Chicago, IL 60637, USA
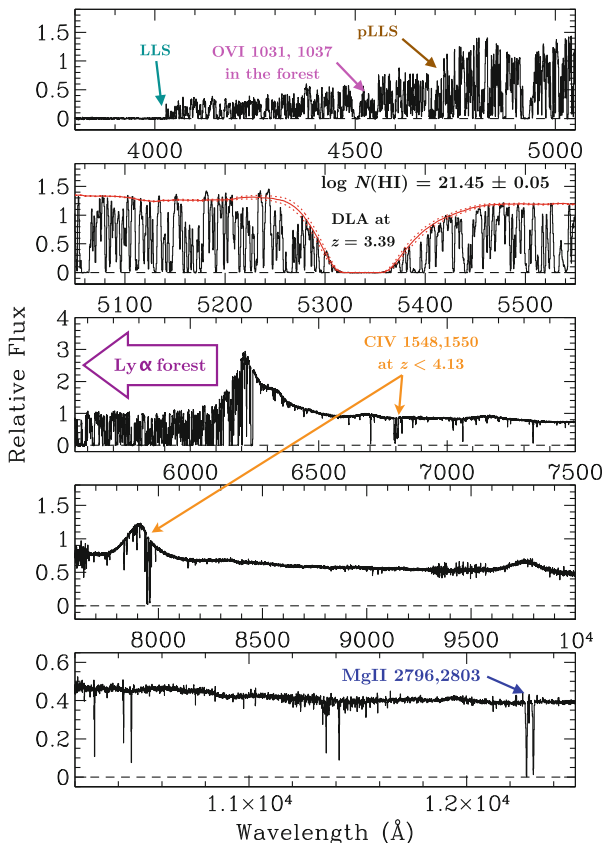e-mail: hchen@oddjob.uchicago.edu

Fig. 9.1 Example of the wealth of information for intervening gas revealed in the optical and near-infrared spectrum of a QSO at $z = 4.13$. In addition to broad emission lines intrinsic to the QSO, such as Lyα/N V at ≈ 6200 Å, a forest of Lyα λ 1215 absorption lines is observed bluewards of 6200 Å. These Lyα forest lines arise in relatively high gas density regions at $z_{abs} \lesssim z_{QSO}$ along the line of sight. The Lyα absorbers span over ten decades in neutral hydrogen column densities ($N(\text{H I})$) and include (1) neutral damped Lyα absorbers (DLAs), (2) optically thick Lyman limit systems (LLS), (3) partial LLS (pLLS) and (4) highly ionized Lyα absorbers (see text for a quantitative definition of these different classes). The DLAs are characterized by pronounced damping wings (*second panel from the top*), while LLS and pLLS are identified based on the apparent flux discontinuities in QSO spectra (*top panel*). Many of these strong Lyα absorbers are accompanied with metal absorption transitions such as the O VI $\lambda\lambda$ 1031, 1037 doublet transitions which occur in the Lyα forest, and the C IV $\lambda\lambda$ 1548, 1550 and Mg II $\lambda\lambda$ 2796, 2803 doublets. Together, these metal lines constrain the ionization state and chemical enrichment of the gas

emission lines are observed, including the Lyα/N V emission at ≈ 6200 Å, C IV emission at ≈ 7900 Å and C III] emission at $\approx$ 9800 Å. Bluewards of the Lyα emission line are a forest of Lyα λ 1215 absorption lines produced by intervening overdense regions at $z_{abs} \lesssim z_{QSO}$ along the QSO sightline. These overdense regions span a wide range in H I column density ($N(\text{H I})$), from neutral interstellar gas of
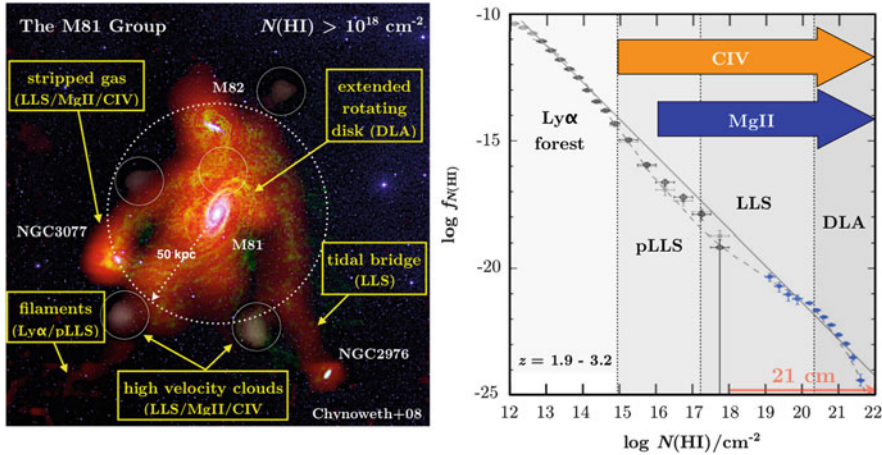
Fig. 9.2 Mapping galaxy outskirts in 21 cm and in QSO absorption-line systems. *Left*: deep 21 cm image of the M81 group, revealing a complex interface between stars and gas in the group. The observed neutral hydrogen column densities range from $N(\mathrm{H\,I}) \sim 10^{18}\,\mathrm{cm}^{-2}$ in the filamentary structures to $N(\mathrm{H\,I}) > 10^{21}\,\mathrm{cm}^{-2}$ in the star-forming disks of group members (Yun et al. 1994; Chynoweth et al. 2008). The 21 cm image reveals a diverse array of gaseous structures in this galaxy group, but these observations become extremely challenging beyond redshift $z \approx 0.2$ (e.g. Verheijen et al. 2007; Fernández et al. 2013). *Right*: The H I column density distribution function of Lyα absorbers, $f_{N(\mathrm{H\,I})}$, uncovered at $z = 1.9$–3.2 along sightlines towards random background QSOs (adapted from Kim et al. 2013). Quasar absorbers in different categories are mapped onto different H I structures both seen and missed in the 21 cm image in the *left panel*. Specifically, DLAs probe the star-forming ISM and extended rotating disks, LLS probe the gaseous streams connecting different group members as well as stripped gas and high-velocity clouds around galaxies and pLLS and strong Lyα absorbers trace ionized gas that is not observed in 21 cm signals. Among the quasar absorbers, C IV absorption transitions are commonly observed in strong Lyα absorbers of $N(\mathrm{H\,I}) \gtrsim 10^{15}\,\mathrm{cm}^{-2}$ (see, e.g. Kim et al. 2013; D'Odorico et al. 2016), and Mg II absorption transitions are seen in most high-$N(\mathrm{H\,I})$ absorbers of $N(\mathrm{H\,I}) \gtrsim 10^{16}\,\mathrm{cm}^{-2}$ (see, e.g. Rigby et al. 2002). These metal-line absorbers trace chemically enriched gas in and around galaxies

$N(\mathrm{H\,I}) \geq 10^{20.3}\,\mathrm{cm}^{-2}$ to optically opaque Lyman limit systems (LLS) of $N(\mathrm{H\,I}) > 10^{17.2}\,\mathrm{cm}^{-2}$, to optically thin partial LLS (pLLS) with $N(\mathrm{H\,I}) = 10^{15-17.2}\,\mathrm{cm}^{-2}$ and to highly ionized Lyα forest lines with $N(\mathrm{H\,I}) = 10^{12-15}\,\mathrm{cm}^{-2}$ (right panel of Fig. 9.2).

The large $N(\mathrm{H\,I})$ in the neutral medium produces pronounced damping wings in the QSO spectrum. These absorbers are commonly referred to as damped Lyα absorbers (DLAs). An example is shown in the second panel from the top in Fig. 9.1. In this particular case, a simultaneous fit to the QSO continuum and the damping wings (red curve in the second panel from the top) yields a best-fit $\log N(\mathrm{H\,I}) = 21.45 \pm 0.05$ for the DLA. At intermediate $N(\mathrm{H\,I})$, LLS and pLLS are identified based on the apparent flux discontinuities in QSO spectra (top panel). A significant fraction of these strong Lyα absorbers have been enriched with heavy elements which produce additional absorption features due to heavy

ions in the QSO spectra. The most prominent features include the O VI $\lambda\lambda$ 1031, 1037 doublet transitions which occur in the Lyα forest and the C IV $\lambda\lambda$ 1548, 1550 and Mg II $\lambda\lambda$ 2796, 2803 doublets, plus a series of low-ionization transitions such as C II, Si II and Fe II. Together, these ionic transitions constrain the ionization state and chemical compositions of the gas (e.g. Chen and Prochaska 2000; Werk et al. 2014).

Combining galaxy surveys with absorption-line observations of gas around galaxies enables comprehensive studies of baryon cycles between star-forming regions and low-density gas over cosmic time. At low redshifts, $z \lesssim 0.2$, deep 21 cm and CO surveys have revealed exquisite details of the cold gas content ($T \lesssim 1000$ K) in nearby galaxies, providing both new clues and puzzles in the overall understanding of galaxy formation and evolution. These include extended H I disks around blue star-forming galaxies with the H I extent $\approx$ 2× what is found for the stellar disk (e.g. Swaters et al. 2002; Walter et al. 2008; Leroy et al. 2008), extended H I and molecular gas in early-type galaxies (e.g. Oosterloo et al. 2010; Serra et al. 2012) with predominantly old stellar populations and little or no ongoing star formation (Salim and Rich 2010) and widespread H I streams connecting regular-looking galaxies in group environments (e.g. Verdes-Montenegro et al. 2001; Chynoweth et al. 2008).

Figure 9.2 (left panel) showcases an example of a deep 21 cm image of the M81 group, a poor group of dynamical mass $M_{dyn} \sim 10^{12} M_{\odot}$ (Karachentsev and Kashibadze 2006). Prominent group members include the grand design spiral galaxy M81 at the centre, the proto-starburst galaxy M82 and several other lower-mass satellites (Burbidge and Burbidge 1961). The 21 cm image displays a diverse array of gaseous structures in the M81 group, from extended rotating disks, warps, high-velocity clouds (HVCs), tidal tails and filaments to bridges connecting what appear to be optically isolated galaxies. High column density gaseous streams of $N(H I) \gtrsim 10^{18}$ cm^{-2} are seen extending beyond 50 kpc in projected distance from M81, despite the isolated appearances of M81 and other group members in optical images. These spatially resolved imaging observations of different gaseous components serve as important tests for theoretical models of galaxy formation and evolution (e.g. Agertz et al. 2009; Marasco et al. 2016). However, 21 cm imaging observations are insensitive to warm ionized gas of $T \sim 10^4$ K and become extremely challenging for galaxies beyond redshift $z = 0.2$ (e.g. Verheijen et al. 2007; Fernández et al. 2013).

QSO absorption spectroscopy extends 21 cm maps of gaseous structures around galaxies to both lower gas column density and higher redshifts. Based on the characteristic $N(H I)$, direct analogues can be drawn between different types of QSO absorbers and different gaseous components seen in deep 21 cm images of nearby galaxies. For example, DLAs probe the neutral gas in the interstellar medium (ISM) and extended rotating disks, LLS probe optically thick gaseous streams and high-velocity clouds in galaxy haloes and pLLS and strong Lyα absorbers of $N(H I) \approx 10^{14-17}$ cm^{-2} trace ionized halo gas and starburst outflows (e.g. supergalactic winds in M 82 Lehnert et al. 1999) that cannot be reached with 21 cm observations.

The right panel of Fig. 9.2 displays the H I column density distribution function, $f_{N(H I)}$, for all Lyα absorbers uncovered at $z = 1.9$–3.2 along random QSO sightlines

(Kim et al. 2013). $f_{N(\mathrm{H\,I})}$, defined as the number of Lyα absorbers per unit absorption path length per unit H I column density interval, is a key statistical measure of the Lyα absorber population. It represents a cross-section weighted surface density profile of hydrogen gas in a cosmological volume. With sufficiently high spectral resolution and high signal-to-noise ratio, $S/N \gtrsim 30$, QSO absorption spectra probe tenuous gas with $N(\mathrm{H\,I})$ as low as $N(\mathrm{H\,I}) \sim 10^{12}\,\mathrm{cm}^{-2}$. The steeply declining $f_{N(\mathrm{H\,I})}$ with increasing $N(\mathrm{H\,I})$ shows that the occurrence (or areal coverage) of pLLS and strong Lyα absorbers of $N(\mathrm{H\,I}) \approx 10^{14-17}\,\mathrm{cm}^{-2}$ is ≈ 10 times higher than that of optically thick LLS along a random sightline and ≈ 100 times higher than the incidence of DLAs. Such a differential frequency distribution is qualitatively consistent with the spatial distribution of H I gas recorded in local 21 cm surveys (e.g. Fig. 9.2, left panel), where gaseous disks with $N(\mathrm{H\,I})$ comparable to DLAs cover a much smaller area on the sky than streams and HVCs with $N(\mathrm{H\,I})$ comparable to LLS. If a substantial fraction of optically thin absorbers originate in galaxy haloes, then their higher incidence implies a gaseous halo of size at least three times what is seen in deep 21 cm images.

In addition, many of these strong Lyα absorbers exhibit associated transitions due to heavy ions. In particular, C IV absorption transitions are commonly observed in strong Lyα absorbers of $N(\mathrm{H\,I}) \gtrsim 10^{15}\,\mathrm{cm}^{-2}$ (see, e.g. Kim et al. 2013; D'Odorico et al. 2016), and Mg II absorption transitions are seen in most high-$N(\mathrm{H\,I})$ absorbers of $N(\mathrm{H\,I}) \gtrsim 10^{16}\,\mathrm{cm}^{-2}$ (e.g. Rigby et al. 2002). While Mg II absorbers are understood to originate in photoionized gas of temperature $T \sim 10^4$ K (e.g. Bergeron and Stasińska 1986), C IV absorbers are more commonly seen in complex, multiphase media (e.g. Rauch et al. 1996; Boksenberg and Sargent 2015). These metal-line absorbers therefore offer additional probes of chemically enriched gas in and around galaxies.

This chapter presents a brief review of the current state of knowledge on the outskirts of distant galaxies from absorption-line studies. The review will first focus on the properties of the neutral gas reservoir probed by DLAs and then outline the insights into star formation and chemical enrichment in the outskirts of distant galaxies from searches of DLA galaxies. A comprehensive review of DLAs is already available in Wolfe et al. (2005). Therefore, the emphasis here focusses on new findings over the past decade. Finally, a brief discussion will be presented on the empirical properties and physical understandings of the ionized circumgalactic gas as probed by strong Lyα and various metal-line absorbers.

9.2 Tracking the Neutral Gas Reservoir over Cosmic Time

DLAs are historically defined as Lyα absorbers with neutral hydrogen column densities exceeding $N(\mathrm{H\,I}) = 2 \times 10^{20}\,\mathrm{cm}^{-2}$ (Wolfe et al. 2005), corresponding to a surface mass density limit of $\Sigma_{\mathrm{atomic}} \approx 2\,M_\odot\,\mathrm{pc}^{-2}$ for atomic gas (including helium). The large gas surface mass densities revealed in high-redshift DLAs are comparable to what is seen in 21 cm observations of nearby star-forming galaxies

(e.g. Walter et al. 2008; Leroy et al. 2008), making DLAs a promising signpost of young galaxies in the distant Universe (Wolfe et al. 1986). In addition, the $N(\text{H I})$ threshold ensures that the gas is neutral under the metagalactic ionizing radiation field (e.g. Viegas 1995; Prochaska and Wolfe 1996; Prochaska et al. 2002). Neutral gas provides the seeds necessary for sustaining star formation. Therefore, observations of DLAs not only help establish a census of the cosmic evolution of the neutral gas reservoir (e.g. Neeleman et al. 2016a) but also offer a unique window into star formation physics in distant galaxies (e.g. Lanzetta et al. 2002; Wolfe and Chen 2006).

While the utility of DLAs for probing the young Universe is clear, these objects are relatively rare (see the right panel of Fig. 9.2), and establishing a statistically representative sample of these rare systems requires a large sample of QSO spectra. Over the last decade, significant progress has been made in characterizing the DLA population at $z \gtrsim 2$, owing to the rapidly growing spectroscopic sample of high-redshift QSOs from the Sloan Digital Sky Survey (SDSS; York et al. 2000). The blue points in the right panel of Fig. 9.2 are based on $\sim$1000 DLAs and $\sim$500 strong LLS identified at $z \approx 2$–5 in an initial SDSS DLA sample (Noterdaeme et al. 2009). The sample of known DLAs at $z \gtrsim 2$ has continued to grow, reaching $\sim$10,000 DLAs found in the SDSS spectroscopic QSO sample (e.g. Noterdaeme et al. 2012).

The large number of known DLAs has led to an accurate characterization of the neutral gas reservoir at high redshifts. Figure 9.3a displays the observed $N(\text{H I})$ distribution function, f_{DLA}, based on $\sim$7000 DLAs identified at $z \approx 2$–5 (Noterdaeme et al. 2012). The plot shows that f_{DLA} is well represented by a Schechter function (Schechter 1976) at $\log N(\text{H I}) \lesssim 22$ following

$$f_{\text{DLA}} \equiv f_{N(\text{H I})}(\log N(\text{H I}) \geq 20.3) \propto \left[\frac{N(\text{H I})}{N_*(\text{H I})} \right]^{\alpha} \exp[-N(\text{H I})/N_*(\text{H I})], \quad (9.1)$$

with a shallow power-law index of $\alpha \approx -1.3$ below the characteristic H I column density $\log N_*(\text{H I}) \approx 21.3$ and a steep exponential decline at larger $N(\text{H I})$ (Noterdaeme et al. 2009, 2012). At $\log N(\text{H I}) > 22$, the observations clearly deviate from the best-fit Schechter function. However, DLAs are also exceedingly rare in this high-$N(\text{H I})$ regime. Only eight such strong DLAs have been found in this large DLA sample (Noterdaeme et al. 2012), making measurements of f_{DLA} in the two highest-$N(\text{H I})$ bins very uncertain. In comparison to $f_{N(\text{H I})}$ established from 21 cm maps of nearby galaxies (Zwaan et al. 2005), the amplitude of f_{DLA} at $z \gtrsim 2$ is $\approx 2\times$ higher than $f_{N(\text{H I})}$ at $z \approx 0$, but the overall shapes are remarkably similar at both low- and high-$N(\text{H I})$ regimes (Fig. 9.3a; see also Sánchez-Ramírez et al. 2016; Rafelski et al. 2016).

At $\log N(\text{H I}) > 21$, numerical simulations have shown that the predicted shape in f_{DLA} is sensitive to the detailed ISM physics, including the formation of molecules (H_2) and different feedback processes (e.g. Altay et al. 2011, 2013; Bird et al. 2014). Comparison of the observed and predicted f_{DLA} therefore provides an independent and critical test for the prescriptions of these physical processes in cosmological simulations. However, the constant exponentially declining trend at
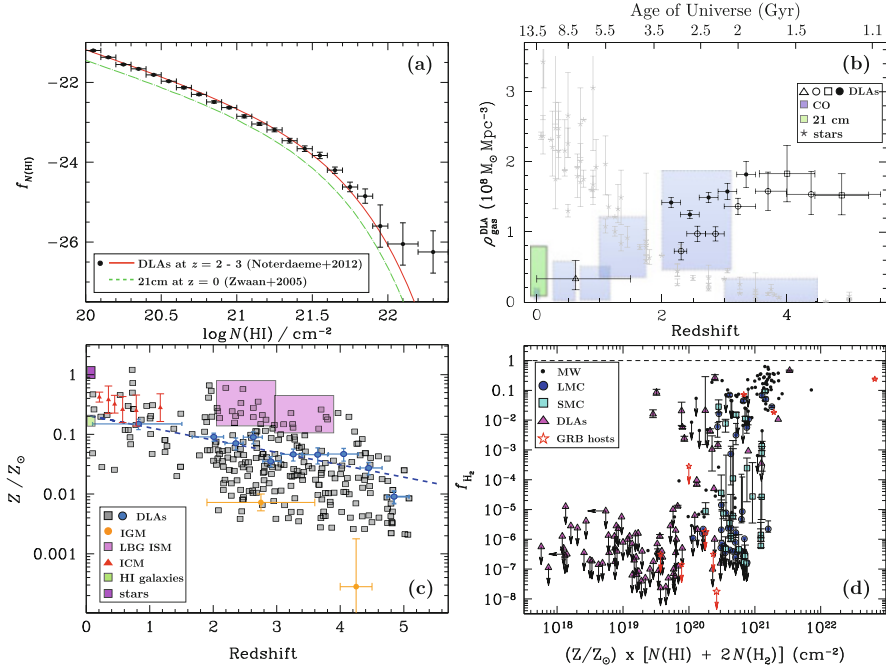
Fig. 9.3 Summary of known DLA properties: (**a**) evolving neutral hydrogen column density distribution functions, $f_{N(\mathrm{H\,I})}$, from DLAs at $z = 2$–3 (Noterdaeme et al. 2012) to H I galaxies at $z \approx 0$ (Zwaan et al. 2005); (**b**) declining cosmic neutral gas mass density with increasing Universe age (or decreasing redshift) from observations of DLAs (*solid points* from Noterdaeme et al. 2012, *open circles* from Prochaska and Wolfe 2009, *open squares* from Crighton et al. 2015 and *open triangle* from Neeleman et al. 2016a) following Eq. (9.2), local H I galaxies (*green-shaded box*, a compilation from Neeleman et al. 2016a) and molecular gas (*blue-shaded boxes*, Decarli et al. 2016), in comparison to increasing cosmic stellar mass density in galaxies with increasing Universe age (*grey asterisks*, a compilation from Madau and Dickinson 2014); (**c**) gas-phase metallicity (Z) relative to Solar ($Z_\odot$) as a function of redshift in DLAs (*grey squares* for individual absorbers and *blue points* for $N(\mathrm{H\,I})$-weighted mean from Marc Rafelski, Rafelski et al. 2012, 2014), IGM at $z \gtrsim 2$ (*orange circles*, Aguirre et al. 2008; Simcoe 2011), ISM of starburst galaxies at $z \approx 2$–4 (*light magenta boxes*, Pettini et al. 2001; Pettini 2004; Erb et al. 2006a; Maiolino et al. 2008; Mannucci et al. 2009), intra-cluster medium in X-ray luminous galaxy clusters at $z \lesssim 1$ (*red triangles*, Balestra et al. 2007), H I-selected galaxies (*green box*, Zwaan et al. 2005) and stars at $z = 0$ (*dark purple box*, Gallazzi et al. 2008); and (**d**) molecular gas fraction, $f_{\mathrm{H_2}}$, versus total surface density of neutral gas scaled by gas metallicity for high-redshift DLAs in *triangles* (Noterdaeme et al. 2008, 2016), γ-ray burst host ISM in *star symbols* (e.g. Noterdaeme et al. 2015) and local ISM in the Milky Way (Wolfire et al. 2008) and Large and Small Magellanic Clouds (Tumlinson et al. 2002) in *dots*, *blue circles* and *cyan squares*, respectively

$N(\mathrm{H\,I}) \gtrsim 2 \times 10^{21} \, \mathrm{cm}^{-2}$ between low-redshift H I galaxies and high-redshift DLAs presents a puzzle.

At $z = 0$, the rapidly declining $f_{N(\mathrm{H\,I})}$ at $N(\mathrm{H\,I}) \gtrsim N_*(\mathrm{H\,I})$ has been interpreted as due to the conversion of atomic gas to molecular gas (Zwaan and Prochaska 2006; Braun 2012). As illustrated at the end of this section and in Fig. 9.3d, the column

density threshold beyond which the gas transitions from H I to H_2 depends strongly on the gas metallicity, and the mean metallicity observed in the atomic gas decreases steadily from $z \approx 0$ to $z > 4$ (Fig. 9.3c). Therefore, the conversion to molecules in high-redshift DLAs is expected to occur at higher $N(\text{H I})$, resulting in a higher $N_*(\text{H I})$ with increasing redshift. However, this is not observed (e.g. Prochaska and Wolfe 2009; Sánchez-Ramírez et al. 2016; Rafelski et al. 2016; Fig. 9.3a). Based on spatially resolved 21 cm maps of nearby galaxies with ISM metallicity spanning over a decade, it has been shown that $f_{N(\text{H I})}$ established individually for these galaxies does not vary significantly with their ISM metallicity (Erkal et al. 2012). Together, these findings demonstrate that the exponential decline of f_{DLA} at $N(\text{H I}) \gtrsim N_*(\text{H I})$ is not due to conversion of H I to H_2, but the physical origin remains unknown.

Nevertheless, the observed f_{DLA} immediately leads to two important statistical quantities: (1) the number density of DLAs per unit survey path length, obtained by integrating f_{DLA} over all $N(\text{H I})$ greater than $N_0 = 2 \times 10^{20}\,\text{cm}^{-2}$, and (2) the cosmic neutral gas mass density, contained in DLAs, Ω_{atomic}, which is the $N(\text{H I})$-weighted integral of f_{DLA} following

$$\Omega_{\text{atomic}} \equiv \rho_{\text{gas}}/\rho_{\text{crit}} = \int_{N_0}^{\infty} (\mu\, H_0/c/\rho_{\text{crit}})\, N(\text{H I})\, f_{\text{DLA}}\, \mathrm{d}\, N(\text{H I}), \qquad (9.2)$$

where $\mu = 1.3$ is the mean atomic weight of the gas particles (accounting for the presence of helium), H_0 is the Hubble constant, c is the speed of light and ρ_{crit} is the critical density of the Universe (e.g. Lanzetta et al. 1991; Wolfe et al. 1995). The shallow power-law index α in the best-fit f_{DLA}, together with a steep exponential decline at high $N(\text{H I})$ from the Schechter function in Eq. (9.1), indicates that while DLAs of $N(\text{H I}) < N_*(\text{H I})$ dominate the neutral gas cross-section (and therefore the number density), strong DLAs of $N(\text{H I}) \sim N_*(\text{H I})$ contribute predominantly to the neutral mass density in the Universe (e.g. Zwaan et al. 2005). A detailed examination of the differential Ω_{atomic} distribution as a function of $N(\text{H I})$ indeed confirms that the bulk of neutral gas is contained in DLAs of $N(\text{H I}) \approx 2 \times 10^{21}\,\text{cm}^{-2}$ (e.g. Noterdaeme et al. 2012).

The cosmic evolution of ρ_{gas} observed in DLAs, from Eq. (9.2), is shown in black points in Fig. 9.3b. Only measurements based on blind DLA surveys are presented in the plot.[1] These include an early sample of ≈ 700 DLAs at $z = 2.5\text{–}5$ in the SDSS Data Release (DR) 5 (open circles; Prochaska and Wolfe 2009), an expanded

---

[1]At $z \lesssim 1.6$, DLA surveys require QSO spectroscopy carried out in space and have been limited to the number of UV-bright QSOs available for absorption-line searches. Consequently, the number of known DLAs from blind surveys is small, ≈ 15 (see Neeleman et al. 2016a for a compilation). To increase substantially the sample of known DLAs at low redshifts, Rao & Turnshek (Rao et al. 2006) devised a clever space programme to search for new DLAs in known Mg II absorbers. Their strategy yielded a substantial gain, tripling the total sample size of $z \lesssim 1.6$ DLAs. However, the Mg II-selected DLA sample also includes a survey bias that is not well understood. It has been shown that excluding Mg II-selected DLAs reduces the inferred Ω_{atomic} by more than a factor of 4 (e.g. Neeleman et al. 2016a). For consistency, only measurements of Ω_{atomic} based on blind DLA surveys are included in the plot.

sample of $\approx$7000 DLAs in the SDSS DR12 (solid points; Noterdaeme et al. 2012), an expanded high-redshift sample of DLAs at $z = 4$–5 (open squares; Crighton et al. 2015) and a sample of $\approx$14 DLAs at $z \lesssim 1.6$ from an exhaustive search in the *Hubble Space Telescope* (*HST*) UV spectroscopic archive (open triangle; Neeleman et al. 2016a).

A range of mean H I mass density at $z \approx 0$ has been reported from different 21 cm surveys (see Neeleman et al. 2016a for a recent compilation). These measurements are included in the green box in Fig. 9.3b. Despite a relatively large scatter between different 21 cm surveys and between DLA surveys, a steady decline in Ω_{atomic} is observed from $z \approx 4$ to $z \approx 0$. For comparison, the cosmic evolution of the molecular gas mass density obtained from a recent blind CO survey (Decarli et al. 2016) is also included as blue-shaded boxes in Fig. 9.3b, along with the cosmic evolution of stellar mass density measured in different galaxy surveys, shown in grey asterisks (data from Madau and Dickinson 2014). Figure 9.3b shows that the decline in the neutral gas mass density with decreasing redshift is coupled with an increase in the mean stellar mass density in galaxies, which is qualitatively consistent with the expectation that neutral gas is being consumed to form stars. However, it is also clear that atomic gas alone is insufficient to explain the observed order of magnitude gain in the total stellar mass density from $z \approx 3$ to $z \approx 0$, which implies the need for replenishing the neutral gas reservoir with accretion from the intergalactic medium (IGM) (e.g. Kereš et al. 2009; Prochaska and Wolfe 2009). At the same time, new blind CO surveys have shown that molecular gas contributes roughly an equal amount of neutral gas mass density as atomic gas observed in DLAs at $z \lesssim 3$ (e.g. Walter et al. 2014; Decarli et al. 2016), although the uncertainties are still very large. Together with the knowledge of an extremely low molecular gas fraction in DLAs (see the discussion on the next page and Fig. 9.3d), these new CO surveys indicate that previous estimates of the total neutral gas mass density based on DLAs alone have been underestimated by as much as a factor of 2. An expanded blind CO survey over a cosmological volume is needed to reduce the uncertainties in the observed molecular gas mass densities at different redshifts, which will cast new insights into the connections between the star formation, the neutral gas reservoir and the ionized IGM over cosmic time.

Observations of the chemical compositions of DLAs provide additional clues to the connection between the neutral gas probed by DLAs and star formation (e.g. Pettini 2004). In particular, because the gas is predominantly neutral, the dominant ionization for most heavy elements (such as Mg, Si, S, Fe, Zn, etc.) is in the singly ionized state, and therefore the observed abundances of these low-ionization species place direct and accurate constraints on the elemental abundances of the gas (e.g. Viegas 1995; Prochaska and Wolfe 1996; Vladilo et al. 2001; Prochaska et al. 2002). Additional constraints on the dust content and on the sources that drive the chemical enrichment history in DLAs can be obtained by comparing the relative abundances of different elements. Specifically, comparing the relative abundances between refractory (such as Cr and Fe) and non-refractory elements (such as S and Zn) indicates the presence of dust in the neutral gas, the amount of which increases with metallicity (e.g. Meyer et al. 1989; Pettini et al. 1990; Savage

and Sembach 1996; Wolfe et al. 2005). The relative abundances of α- to Fe-peak elements determine whether core-collapse supernovae (SNe) or SNe Ia dominate the chemical enrichment history, and DLAs typically exhibit an α-element-enhanced abundance pattern (e.g. Lu et al. 1996; Pettini et al. 1999; Prochaska and Wolfe 1999).

Figure 9.3c presents a summary of gas metallity (Z) relative to Solar ($Z_\odot$) measured for >250 DLAs at $z \lesssim 5$ (grey squares from Rafelski et al. 2012, 2014). The cosmic mean gas metallicity in DLAs as a function of redshift can be determined based on a $N(\text{H\,I})$-weighted average over an ensemble of DLAs in each redshift bin (blue points), which is found to increase steadily with decreasing redshift following a best-fit mean relation of $\langle Z/Z_\odot \rangle = [-0.20 \pm 0.03]\,z - [0.68 \pm 0.09]$ (dashed blue line, Rafelski et al. 2014). For comparison, the figure also includes measurements for stars (dark purple box, Gallazzi et al. 2008) and H\,I-selected galaxies (green box, Zwaan et al. 2005) at $z = 0$, iron abundances in the intra-cluster medium in X-ray luminous galaxy clusters at $z \lesssim 1$ (red triangles, Balestra et al. 2007), ISM of starburst galaxies (light magenta boxes) at $z \approx 2$–3 (Pettini et al. 2001; Pettini 2004; Erb et al. 2006a) and at $z = 3$–4 (Maiolino et al. 2008; Mannucci et al. 2009) and IGM at $z \gtrsim 2$ (orange circles, Aguirre et al. 2008; Simcoe 2011).

It is immediately clear from Fig. 9.3c that there exists a large scatter in the observed metallicity in DLAs at all redshifts. In addition, while the cosmic mean metallicity in DLAs is significantly higher than what is observed in the low-density IGM, it remains lower than what is observed in the star-forming ISM at $z = 2$–4 and a factor of ≈ 5 below the mean values observed in stars at $z = 0$. The chemical enrichment level in DLAs is also lower than the iron abundances seen in the intra-cluster medium at intermediate redshifts. The observed low metallicity relative to the measurements in and around known luminous galaxies raised the question of whether or not the DLAs probe preferentially low-metallicity, gas-rich galaxies and are not representative of more luminous, metal-rich galaxies found in large-scale surveys (e.g. Pettini 2004).

The large scatter in the observed metallicity in DLAs is found to be explained by a combination of two factors (Chen et al. 2005): (1) the mass-metallicity (or luminosity-metallicity) relation in which more massive galaxies on average exhibit higher global ISM metallicities (e.g. Tremonti et al. 2004; Erb et al. 2006a; Neeleman et al. 2013; Christensen et al. 2014) and (2) metallicity gradients commonly seen in star-forming disks with lower metallicities at larger distances (e.g. Zaritsky et al. 1994; van Zee et al. 1998; Sánchez et al. 2014; Wuyts et al. 2016). If DLAs sample a representative galaxy population including both low-mass and massive galaxies and probe both inner and outer disks of these galaxies, then a large metallicity spread is expected.

The observed low metallicity in DLAs, relative to star-forming ISM, is also understood as due to a combination of DLAs being a gas cross-section selected sample and the presence of metallicity gradients in disk galaxies (Chen et al. 2005). A cross-section selected sample contains a higher fraction of absorbers originating in galaxy outskirts than in the inner regions, and the presence of metallicity gradients

indicates that galaxy outskirts have lower metallicities than what is observed in inner disks (see Sect. 9.3 and Fig. 9.4 below for more details). Indeed, including both factors, a gas cross-section weighting scheme and a metallicity gradient, for local H I galaxies resulted in a mean metallicity comparable to what is observed in DLAs (green box in Fig. 9.3c; Zwaan et al. 2005).

While DLAs exhibit a moderate level of chemical enrichment, searches for molecular gas in DLAs have yielded only a few detections (e.g. Noterdaeme et al. 2008, 2016; Jorgenson et al. 2014). Figure 9.3d displays the observed molecular gas fraction, which is defined as $f_{H_2} \equiv 2 N(H_2)/[N(H I) + 2 N(H_2)]$, versus metallicity-scaled total hydrogen column density for ≈100 DLAs at $z \approx$ 2–4 (triangles). The DLAs span roughly two decades in $N(H I)$ from $N(H I) \approx 2 \times 10^{20}$ cm^{-2} to
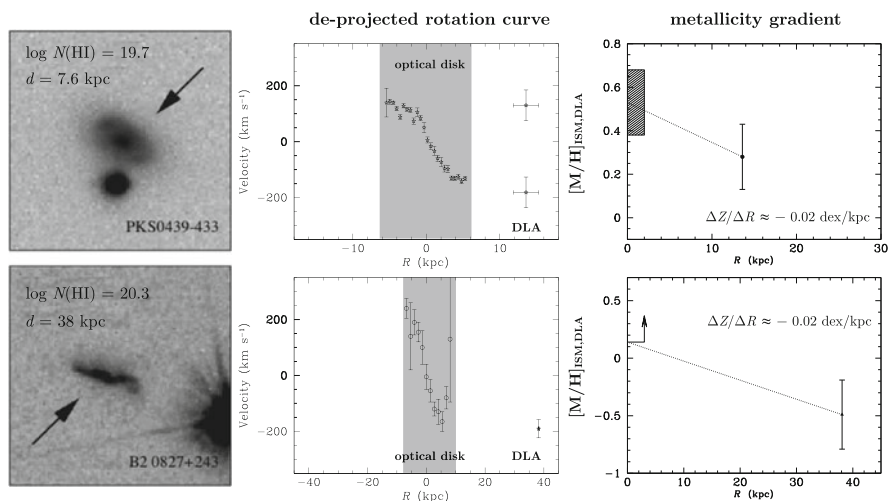

Fig. 9.4 Neutral gas kinematics and metallicity revealed by the presence of a DLA in the outskirts of two L_* galaxies (adapted from Chen et al. 2005). The *top row* presents a DLA found at $d = 7.6$ kpc from a disk galaxy at $z = 0.101$, which also exhibits widespread CO emission in the disk (Neeleman et al. 2016b). The *bottom row* presents a DLA at $d = 38$ kpc from an edge-on disk at $z = 0.525$. Deep *r*-band images of the galaxies are presented in the *left panels*, which display spatially resolved disk morphologies and enable accurate measurements of the inclination and orientation of the optical disk. The *middle panels* present the optical rotation curves deprojected along the disk plane (points in shaded area) based on the inclination angle determined from the optical image of each galaxy (Eqs. (9.3) and (9.4)). If the DLAs occur in extended disks, the corresponding galactocentric distances of the two galaxies from Eq. (9.3) are $R = 13.6$ kpc (*top*) and $R = 38$ kpc (*bottom*). The DLA in the *top panel* is resolved into two components of comparable ionic column densities (Som et al. 2015) but an order of magnitude difference in $N(H_2)$ (Muzahid et al. 2015). The component with a lower $N(H_2)$ appears to be corotating with the optical disk (lower DLA data point), while the component with stronger $N(H_2)$ appears to be counterrotating, possibly due to a satellite (upper DLA data point). The DLA in the *bottom panel* displays simpler gas kinematics consistent with an extended rotating disk out to ≈40 kpc. The *right panels* present the metallicity gradient observed in the gaseous disks based on comparisons of ISM gas-phase metallicity and metallicity of the DLA beyond the optical disks. In both cases, the gas metallicity declines with increasing radius according to $\Delta Z/\Delta R = -0.02$ dex kpc^{-1}

$N(\text{H\,I}) \approx 2.5 \times 10^{22}\,\text{cm}^{-2}$. Strong limits have been placed for f_{H_2} for the majority of DLAs at $f_{\text{H}_2} \lesssim 10^{-5}$ with only $\approx 10\%$ displaying the presence of H_2 and two having $f_{\text{H}_2} > 0.1$. In contrast, the ISM of the Milky Way (MW), at comparable $N(\text{H\,I})$, displays a much higher f_{H_2} than the DLAs at high redshifts.

The formation of molecules is understood to depend on two competing factors: (1) the ISM radiation field which photodissociates molecules and (2) dust which facilitates molecule formation (e.g. Elmegreen 1993; Cazaux and Spaans 2004). Dust is considered a more dominant factor because of its dual roles in both forming molecules and shielding them from the ISM radiation field. In star-forming galaxies, the dust-to-gas mass ratio is observed to correlate strongly with ISM gas-phase metallicity (e.g. Leroy et al. 2011; Rémy-Ruyer et al. 2014). It is therefore expected that the observed molecular gas fraction should correlate with gas metallicity (e.g. Elmegreen 1989; Krumholz et al. 2009; Gnedin et al. 2009).

In the MW ISM with metallicity roughly Solar, $Z \approx Z_\odot$, the molecular gas fraction is observed to increase sharply from $f_{\text{H}_2} < 10^{-4}$ to $f_{\text{H}_2} \gtrsim 0.1$ at $N(\text{H\,I}) \approx 2 \times 10^{20}\,\text{cm}^{-2}$ (see Wolfire et al. 2008). The sharp transition from atomic to molecular is also observed in the ISM of the Large and Small Magellanic Clouds (LMC and SMC), but occurs at higher gas column densities of $N(\text{H\,I}) \approx 10^{21}\,\text{cm}^{-2}$ for the LMC and $N(\text{H\,I}) \approx 3 \times 10^{21}\,\text{cm}^{-2}$ for the SMC (see Tumlinson et al. 2002). The ISM metallicities of LMC and SMC are $Z \approx 0.5\,Z_\odot$ and $Z \approx 0.15\,Z_\odot$, respectively. These observations therefore support a simple metallicity-dependent transitional gas column density illustrated in Fig. 9.3d. Following the metallicity-scaling relation, it is clear that despite a high $N(\text{H\,I})$, most DLAs do not have sufficiently high metallicity (and therefore dust content) to facilitate the formation of molecules (Gnedin and Kravtsov 2010; Gnedin and Draine 2014; Noterdaeme et al. 2015). This finding also applies to γ-ray burst (GRB) host galaxies (star symbols in Fig. 9.3d). With few exceptions (Prochaska et al. 2009; Krühler et al. 2013; Friis et al. 2015), the ISM in most GRB hosts displays a combination of very high $N(\text{H\,I})$ and low f_{H_2} (e.g. Tumlinson et al. 2007; Ledoux et al. 2009). The observed absence of H_2 in DLAs, together with a large molecular mass density revealed in blind CO surveys (e.g. Walter et al. 2014; Decarli et al. 2016), shows that a complete census for the cosmic evolution of the neutral gas reservoir requires complementary surveys of molecular gas over a broad redshift range. In addition, as described in Sect. 9.4 below, the observed low molecular gas content also has important implications for star formation properties in metal-deficient, high neutral gas surface density environments.

9.3 Probing the Neutral Gas Phase in Galaxy Outskirts

Considerable details have been learned about the physical properties and chemical enrichment in neutral atomic gas from DLA studies. To apply the knowledge of DLAs for a better understanding of distant galaxies, it is necessary to first identify

DLA galaxies and compare them with the general galaxy population. Searches for DLA galaxies are challenging, because distant galaxies are faint and because the relatively small extent of high-N(H I) gas around galaxies places the absorbing galaxies at small angular distances from the bright background QSOs. Based on a well-defined H I size-mass relation observed in local H I galaxies (e.g. Broeils and Rhee 1997; Verheijen and Sancisi 2001; Swaters et al. 2002), the characteristic projected separation (accounting for weighting by cross-section) between a DLA and an L_* absorbing galaxy is $\approx$16 kpc and smaller for lower-mass galaxies. At $z = 1$–2, a projected distance of 16 kpc corresponds to an angular separation of $\lesssim 2''$ and greater at lower and higher redshifts.

While fewer DLAs are known at $z \lesssim 1$ (see Sect. 9.2), a large number ($\approx$40) of these low-redshift DLAs have their galaxy counterparts (or candidates) found based on a combination of photometric and spectroscopic techniques (e.g. Chen and Lanzetta 2003; Rao et al. 2003, 2011; Péroux et al. 2016). It has been shown based on this low-redshift DLA galaxy sample that DLAs probe a representative galaxy population in luminosity and colour. DLA galaxies are consistent with an H I cross-section selected sample with a large fraction of DLAs found at projected distance $d \gtrsim 10$ kpc from the absorbing galaxies (e.g. Chen and Lanzetta 2003; Rao et al. 2011). In addition to regular disk galaxies, two DLAs have been found in a group environment (e.g. Bergeron and Boissé 1991; Chen and Lanzetta 2003; Kacprzak et al. 2010; Péroux et al. 2011), suggesting that stripped gas from galaxy interactions could also contribute to the incidence of DLAs. The low-redshift DLA sample is expected to continue to grow dramatically with new discoveries from the SDSS (e.g. Straka et al. 2015). In contrast, the search for DLA galaxies at $z > 2$ has been less successful despite extensive efforts (e.g. Warren et al. 2001; Møller et al. 2002; Péroux et al. 2012; Fumagalli et al. 2015). To date, only $\approx$12 DLA galaxies have been found at $z > 2$ (Krogager et al. 2012; Fumagalli et al. 2015).

In addition to a general characterization of the DLA galaxy population, individual DLA and galaxy pairs provide a unique opportunity to probe neutral gas in the outskirts of distant galaxies. Figure 9.4 shows two examples of constraining the kinematics and chemical enrichment in the outskirts of neutral disks from combining resolved optical imaging and spectroscopy of the galaxy with an absorption-line analysis of the DLA. In the first example (top row), a DLA of log N(H I) $= 19.7$ is found at $d = 7.6$ kpc from an L_* galaxy at $z = 0.101$, which also exhibits widespread CO emission in the disk (Neeleman et al. 2016b). The galaxy disk is resolved in the ground-based r-band image (upper-left panel), which enables accurate measurements of the disk inclination and orientation (Chen et al. 2005). While the observed N(H I) falls below the nominal threshold of a DLA, the gas is found to be largely neutral (e.g. Chen et al. 2005; Som et al. 2015). In addition, abundant H_2 is detected in the absorbing gas (Muzahid et al. 2015). Optical spectra of the galaxy clearly indicate a strong velocity shear along the disk, suggesting an organized rotation motion (Chen et al. 2005) which is confirmed by recent CO observations (Neeleman et al. 2016b). At the same time, the DLA is resolved into two components of comparable ionic column densities (Som et al. 2015) but an order of magnitude difference in $N(H_2)$ (Muzahid et al. 2015). A rotation curve

of the gaseous disk extending beyond 10 kpc (top-centre panel) can be established based on the observed velocity shear (v_{obs}) and deprojection onto the disk plane following

$$\frac{R}{d} = \sqrt{1 + \sin^2(\phi)\tan^2(i)} \tag{9.3}$$

and

$$v = \frac{v_{obs}}{\cos(\phi)\sin(i)}\sqrt{1 + \sin^2(\phi)\tan^2(i)}, \tag{9.4}$$

where R is the galactocentric radius along the disk, v is the deprojected rotation velocity, i is the inclination angle of the disk and ϕ is the azimuthal angle from the major axis of the disk where the DLA is detected (Chen et al. 2005; see also Steidel et al. 2002 for an alternative formalism). For the two absorbing components in this DLA, it is found that the component with a lower $N(H_2)$ appears to be corotating with the optical disk (lower DLA data point), while the component with stronger $N(H_2)$ appears to be counterrotating, possibly due to a satellite (upper DLA data point). Comparing the ISM gas-phase metallicity and the metallicity of the DLA shows a possible gas metallicity gradient of $\Delta Z/\Delta R = -0.02$ dex kpc^{-1} out to $R \approx 14$ kpc.

The bottom row of Fig. 9.4 presents a DLA at $d = 38$ kpc from an edge-on disk at $z = 0.525$. A strong velocity shear is also seen along the disk of this L_* galaxy. Because the QSO sightline occurs along the extended edge-on disk, Eqs. (9.3) and (9.4) directly lead to $R \approx d$ and $v \approx v_{obs}$ for this system. This DLA galaxy presents a second example for galaxies with an extended rotating disk out to ≈ 40 kpc. At the same time, the deep r-band image (lower-left panel) from *HST* suggests that the disk is warped near the QSO sightline, which is also reflected by the presence of a disturbed rotation velocity at $R > 5$ kpc (bottom-centre panel). The metallicity measured in the gas phase (bottom-right panel) displays a similar gradient of $\Delta Z/\Delta R = -0.02$ dex kpc^{-1} to the galaxy at the top, which is also comparable to what is seen in the ISM of nearby disk galaxies (e.g. Zaritsky et al. 1994; van Zee et al. 1998; Sánchez et al. 2014). A declining gas-phase metallicity from the inner ISM to neutral gas at larger distances appears to hold for most DLA galaxies at $z \lesssim 1$, and the declining trend continues into ionized halo gas traced by strong LLS of $N(H\,I) = 10^{19-20}$ cm^{-2} (e.g. Péroux et al. 2016).

At $z > 2$, spatially resolved observations of ISM gas kinematics become significantly more challenging, because the effective radii of L_* galaxies are typically $r_e = 1$–3 kpc (e.g. Law et al. 2012), corresponding to $\lesssim 0.3''$, and smaller for fainter or lower-mass objects. Star-forming regions in these distant galaxies are barely resolved in ground-based, seeing-limited observations (e.g. Law et al. 2007; Förster Schreiber et al. 2009; Wright et al. 2009). Beam smearing can result in significant bias in interpreting the observed velocity shear and distributions of heavy elements (e.g. Davies et al. 2011; Wuyts et al. 2016). However, accurate

measurements can be obtained to differentiate ISM metallicities of DLA galaxies from metallicities of neutral gas beyond the star-forming regions. Using the small sample of known DLA galaxies at $z \gtrsim 2$, a metallicity gradient of $\Delta Z / \Delta R = -0.02$ dex kpc^{-1} is also found in these distant star-forming galaxies (Christensen et al. 2014; Jorgenson and Wolfe 2014).

9.4 The Star Formation Relation in the Early Universe

While direct identifications of galaxies giving rise to $z > 2$ DLAs have proven extremely challenging, critical insights into the star formation relation in the early Universe can still be gained from comparing the incidence of DLAs with the spatial distribution of star formation rate (SFR) per unit area uncovered in deep imaging data (Lanzetta et al. 2002; Wolfe and Chen 2006). Specifically, the SFR per unit area (Σ_{SFR}) is correlated with the surface mass density of neutral gas (Σ_{gas}), following a Schmidt-Kennicutt relation in nearby galaxies (e.g. Schmidt 1959; Kennicutt 1998). The global star formation relation, $\Sigma_{SFR} = 2.5 \times 10^{-4} (\Sigma_{gas}/1\,M_\odot\,\mathrm{pc}^{-2})^{1.4}\,M_\odot\,\mathrm{yr}^{-1}\,\mathrm{kpc}^{-2}$ (dashed line in Fig. 9.5), is established using a sample of local spiral galaxies and nuclear starbursts (solid grey points in Fig. 9.5) over a broad range of Σ_{gas}, from $\Sigma_{gas} \approx 10\,M_\odot\,\mathrm{pc}^{-2}$ to $\Sigma_{gas} \approx 10^4\,M_\odot\,\mathrm{pc}^{-2}$.

Empirical constraints for a Schmidt-Kennicutt relation at high redshifts require observations of the neutral gas content in star-forming galaxies. Although observations of individual galaxies in H I emission remain out of reach, the sample of $z = 1$–3 galaxies with resolved CO maps is rapidly growing (e.g. Baker et al. 2004; Genzel et al. 2010; Tacconi et al. 2013). The observed Σ_{SFR} versus $\Sigma_{molecular}$ for the high-redshift CO-detected sample is shown in open squares in Fig. 9.5, which occur at high surface densities of $\Sigma_{molecular} \gtrsim 100\,M_\odot\,\mathrm{pc}^{-2}$. Considering only $\Sigma_{molecular}$ is appropriate for these galaxies, because locally it has been shown that at this high surface density regime, molecular gas dominates (e.g. Martin and Kennicutt 2001; Wong and Blitz 2002; Bigiel et al. 2008). In contrast, DLAs probe neutral gas with $N(\mathrm{H\,I})$ ranging from $N(\mathrm{H\,I}) = 2 \times 10^{20}\,\mathrm{cm}^{-2}$ to $N(\mathrm{H\,I}) \approx 5 \times 10^{22}\,\mathrm{cm}^{-2}$. The range in $N(\mathrm{H\,I})$ corresponds to a range in surface mass density of atomic gas from $\Sigma_{atomic} \approx 2\,M_\odot\,\mathrm{pc}^{-2}$ to $\Sigma_{atomic} \gtrsim 200\,M_\odot\,\mathrm{pc}^{-2}$, which is comparable to the global average of total neutral gas surface mass density in local disk galaxies (e.g. Fig. 9.5). Therefore, DLAs offer an important laboratory for investigating the star formation relation in the distant Universe, and direct constraints can be obtained from searches of in situ star formation in DLAs.

In principle, the Schmidt-Kennicutt relation can be rewritten in terms of $N(\mathrm{H\,I})$ for pure atomic gas following

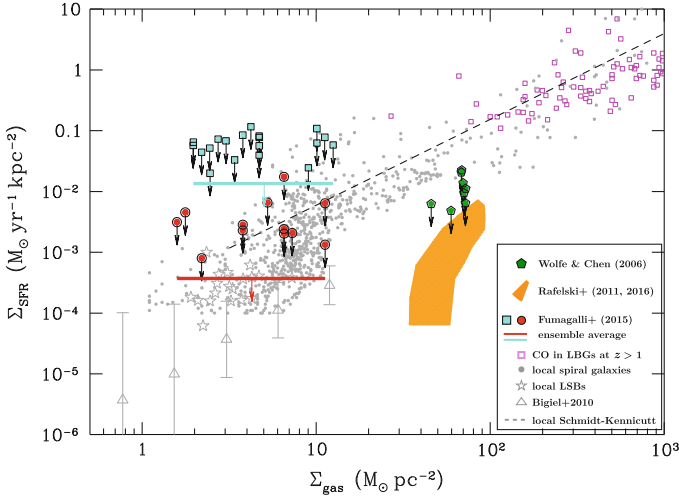$$\Sigma_{SFR} = K \times [N(\mathrm{H\,I})/N_0]^\beta \quad M_\odot\,\mathrm{yr}^{-1}\,\mathrm{kpc}^{-2}, \tag{9.5}$$

Fig. 9.5 The global star formation relation observed in nearby galaxies and at high redshifts. The correlation between the SFR per unit area (Σ_{SFR}) and the total surface gas mass density (Σ_{gas}), combining both atomic (H I) and molecular (H$_2$) for nearby spiral and starburst galaxies, is shown in *small filled circles* (Kennicutt 1998; Graciá-Carpio et al. 2008; Leroy et al. 2008), together with the best-fit Schmidt-Kennicutt relation shown by the *dashed line* (Kennicutt 1998). A reduced star formation efficiency is observed both in low surface brightness galaxies and in the outskirts of normal spirals, which are shown in *grey star symbols* and *open triangles*, respectively (Wyder et al. 2009; Bigiel et al. 2010). CO molecules have been detected in many massive starburst galaxies ($M_{star} > 2.5 \times 10^{10}\, M_\odot$) at $z = 1$–3 (e.g. Baker et al. 2004; Genzel et al. 2010; Tacconi et al. 2013), which occur at the high surface density regime of the global star formation relation (*open squares*). In contrast, searching for in situ star formation in DLAs has revealed a reduced star formation efficiency in this metal-deficient gas. Specifically, *green points* and *orange-shaded area* represent the constraints obtained from comparing the sky coverage of low surface brightness emission with the incidence of DLAs (Wolfe and Chen 2006; Rafelski et al. 2011, 2016). *Cyan squares and red circles* represent the limits inferred from imaging searches of galaxies associated with individual DLAs, and the *cyan and red bars* represent the limiting Σ_{SFR} based on ensemble averages of the two samples (Fumagalli et al. 2015). The level of star formation observed in high-N(H I) DLAs (*green pentagons and orange-shaded* area) is comparable to what is seen in nearby low surface brightness galaxies and in the outskirts of normal spirals. See the main text for a detailed discussion

which is justified for regions probed by DLAs with a low molecular gas content (see Sect. 9.2 and Fig. 9.3d). For reference, the local Schmidt-Kennicutt relation has $K = 2.5 \times 10^{-4}\, M_\odot\, yr^{-1}\, kpc^{-2}$, $\beta = 1.4$ and $N_0 = 1.25 \times 10^{20}\, cm^{-2}$ for a pure atomic hydrogen gas. Following Eq. (9.5), the N(H I) distribution function, $f_{N(H I)}$ (e.g. Fig. 9.3a), can then be expressed in terms of the Σ_{SFR} distribution function, $h(\Sigma_{SFR})$, which is the projected proper area per $d\Sigma_{SFR}$ interval per comoving volume (Lanzetta et al. 2002). The Σ_{SFR} distribution function $h(\Sigma_{SFR})$ is related to $f_{N(H I)}$ according to $h(\Sigma_{SFR})\, d\Sigma_{SFR} = (H_0/c) f_{N(H I)}\, dN(H I)$.

This exercise immediately leads to two important observable quantities. First, the sky covering fraction (C_A) of star-forming regions in the redshift range, $[z_1, z_2]$,

with an observed SFR per unit area in the interval of Σ_{SFR} and $\Sigma_{SFR} + d\Sigma_{SFR}$ is determined following

$$C_A[\Sigma_{SFR}|N(H\,\textsc{i})] = \int_{z_1}^{z_2} \frac{c\,(1+z)^2}{H(z)} h(\Sigma_{SFR})\,d\Sigma_{SFR}\,dz, \tag{9.6}$$

where c is the speed of light and $H(z)$ is the Hubble expansion rate. Equation (9.6) is equivalent to $f_{N(H\,\textsc{i})}dN(H\,\textsc{i})dX$, where $dX \equiv (1+z)^2 H_0/H(z)\,dz$ is the comoving absorption path length. In addition, the first moment of $h(\Sigma_{SFR})$ leads to the comoving SFR density (Lanzetta et al. 2002; Hopkins et al. 2005),

$$\dot{\rho}_*(>\Sigma_{SFR}^{min}) = \int_{\Sigma_{SFR}^{min}}^{\Sigma_{SFR}^{max}} \Sigma_{SFR} h(\Sigma_{SFR})\,d\Sigma_{SFR}. \tag{9.7}$$

Constraints on the star formation relation at high redshift, namely, K and β in Eq. (9.5), can then be obtained by comparing $f_{N(H\,\textsc{i})}$-inferred C_A and $\dot{\rho}_*$ with results from searches of low surface brightness emission in deep galaxy survey data. Furthermore, estimates of missing light in low surface brightness regions can also be obtained using Eq. (9.7) (e.g. Lanzetta et al. 2002; Rafelski et al. 2011).

In practice, Eq. (9.5) is a correct representation only if disks are not well formed and a spherical symmetry applies to the DLAs. For randomly oriented disks, corrections for projection effects are necessary, and detailed formalisms are presented in Wolfe and Chen (2006) and Rafelski et al. (2011). In addition, the inferred surface brightness of in situ star formation in the DLA gas is extremely low after accounting for the cosmological surface brightness dimming. At $z = 2$–3, only DLAs at the highest-$N(H\,\textsc{i})$ end of $f_{N(H\,\textsc{i})}$ are expected to be visible in ultra-deep imaging data (cf. Lanzetta et al. 2002; Wolfe and Chen 2006). For example, DLAs of $N(H\,\textsc{i}) > 1.6 \times 10^{21}\,cm^{-2}$ at $z \approx 3$ are expected to have V-band (corresponding roughly to rest-frame 1500 Å at $z = 3$) surface brightness $\mu_V \lesssim 28.4\,mag\,arcsec^{-2}$, assuming the local Schmidt-Kennicutt relation. The expected low surface brightness of UV photons from young stars in high-redshift DLAs dictates the galaxy survey depth necessary to uncover star formation associated with the DLA gas. At $N(H\,\textsc{i}) > 1.6 \times 10^{21}\,cm^{-2}$, roughly 3% of the sky ($C_A \approx 0.03$) is expected to be covered by extended low surface brightness emission of $\mu_V \lesssim 28.4\,mag\,arcsec^{-2}$. For comparison, the sky covering fraction of luminous starburst galaxies at $z = 2$–3 is less than 0.1%.

Available constraints for the star formation efficiency at $z = 1$–3 are shown in colour symbols in Fig. 9.5. Specifically, the Hubble Ultra-Deep Field (HUDF; Beckwith et al. 2006) V-band image offers sufficient depth for detecting objects of $\mu_V \approx 28.4\,mag\,arcsec^{-2}$. Under the assumption that DLAs originate in regions distinct from known star-forming galaxies, an exhaustive search for extended low surface brightness emission in the HUDF has uncovered only a small number of

these faint objects, far below the expectation from applying the local Schmidt-Kennicutt relation for DLAs of $N(\text{H\,I}) > 1.6 \times 10^{21}\,\text{cm}^{-2}$ following Eq. (9.6). Consequently, matching the observed limit on $\dot{\rho}_*$ from these faint objects with expectations from Eq. (9.7) has led to the conclusion that the star formation efficiency in metal-deficient atomic gas is more than $10\times$ lower than expectations from the local Schmidt-Kennicutt relation (Wolfe and Chen 2006; green pentagons in Fig. 9.5).

On the other hand, independent observations of DLA galaxies at $z = 2$–3 have suggested that these absorbers are associated with typical star-forming galaxies at high redshifts. These include a comparable clustering amplitude of DLAs and these galaxies (e.g. Cooke et al. 2006), the findings of a few DLA galaxies with mass and SFR comparable to luminous star-forming galaxies found in deep surveys (e.g. Møller et al. 2002, 2004; Christensen et al. 2007) and detections of a DLA feature in the ISM of star-forming galaxies (e.g. Pettini et al. 2002; Chen et al. 2009; Dessauges-Zavadsky et al. 2010). If DLAs originate in neutral gas around known star-forming galaxies, then these luminous star-forming galaxies should be more spatially extended than has been realized. Searches for low surface brightness emission in the outskirts of these galaxies based on stacked images have indeed uncovered extended low surface brightness emission out to more than twice the optical extent of a single image. However, repeating the exercise of computing the cumulative $\dot{\rho}_*$ from Eq. (9.7) has led to a similar conclusion that the star formation efficiency is more than $10\times$ lower in metal-deficient atomic gas at $z = 1$–3 than expectations from the local Schmidt-Kennicutt relation (Rafelski et al. 2011, 2016). The results are shown as the orange-shaded area in Fig. 9.5. In addition, the amount of missing light in the outskirts of these luminous star-forming galaxies is found to be $\approx 10\%$ of what is observed in the core (Rafelski et al. 2011).

At the same time, imaging searches of individual DLA galaxies have been conducted for ≈ 30 DLAs identified along QSO sightlines that have high-redshift LLS serving as a natural coronagraph to block the background QSO glare, improving the imaging depth in areas immediate to the QSO sightline (Fumagalli et al. 2015). These searches have yielded only null results, leading to upper limits on the underlying surface brightness of the DLA galaxies (cyan squares and red circles in Fig. 9.5). While the survey depth is not sufficient for detecting associated star-forming regions in most DLAs in the survey sample of Fumagalli et al. (2015) based on the local Schmidt-Kennicutt relation, the ensemble average is beginning to place interesting limits (cyan and red arrows).

The lack of in situ star formation in DLAs may not be surprising given the low molecular gas content. In the local Universe, it is understood that the Schmidt-Kennicutt relation is driven primarily by molecular gas mass ($\Sigma_{\text{molecular}}$), while the surface density of atomic gas (Σ_{atomic}) "saturates" at $\sim 10\,M_\odot\,\text{pc}^{-2}$ beyond which the gas transitions into the molecular phase (e.g. Martin and Kennicutt 2001; Wong and Blitz 2002; Bigiel et al. 2008). As described in Sect. 9.2 and Fig. 9.3d, the transitional surface density from atomic to molecular is metallicity

dependent. Therefore, the low star formation efficiency observed in DLA gas can be understood as a metallicity-dependent Schmidt-Kennicutt relation. This is qualitatively consistent with the observed low Σ_{SFR} in nearby low surface brightness galaxies (e.g. Wyder et al. 2009; star symbols in Fig. 9.5) and in the outskirts of normal spirals (e.g. Bigiel et al. 2010; open triangles in Fig. 9.5), where the ISM is found to be metal-poor (e.g. McGaugh 1994; Zaritsky et al. 1994; Bresolin et al. 2012). Numerical simulations incorporating a metallicity dependence in the H_2 production rate have also confirmed that the observed low star formation efficiency in DLAs can be reproduced in metal-poor gas (e.g. Gnedin and Kravtsov 2010).

A metallicity-dependent Schmidt-Kennicutt relation has wide-ranging implications in extragalactic research, from the physical origin of DLAs at high redshifts to star formation and chemical enrichment histories in different environments and to detailed properties of distant galaxies such as morphologies, sizes and cold gas content. It is clear from Fig. 9.5 that there exists a significant gap in the gas surface densities, between $\Sigma_{\text{gas}} \approx 10\,M_\odot\,\text{pc}^{-2}$ probed by these direct DLA galaxy searches and $\Sigma_{\text{gas}} \approx 100\,M_\odot\,\text{pc}^{-2}$ probed by CO observations of high-redshift starburst systems (open squares in Fig. 9.5). Continuing efforts targeting high-$N(\text{H\,I})$ DLAs (and therefore high Σ_{gas}) at sufficient imaging depths are expected to place critical constraints on the star formation relation in low-metallicity environments at high redshifts. Similarly, spatially resolved maps of star formation and neutral gas at $z > 1$ to mean surface densities of $\Sigma_{\text{SFR}} < 0.1\,M_\odot\,\text{yr}^{-1}\,\text{kpc}^{-2}$ and $\Sigma_{\text{atomic, molecular}} \approx 10-100\,M_\odot\,\text{pc}^{-2}$ will bridge the gap of existing observations and offer invaluable insights into the star formation relation in different environments.

9.5 From Neutral ISM to the Ionized Circumgalactic Medium

Beyond the neutral ISM, strong Lyα absorbers of $N(\text{H\,I}) \approx 10^{14-20}\,\text{cm}^{-2}$ and associated metal-line absorbers offer a sensitive probe of the diffuse circumgalactic medium (CGM) to projected distances $d \approx 100\text{--}500\,\text{kpc}$ (e.g. Fig. 9.2). But because the circumgalactic gas is significantly more ionized in the LLS and lower-$N(\text{H\,I})$ regime, measurements of its ionization state and metallicity bear considerable uncertainties and should be interpreted with caution.

Several studies have attempted to constrain the ionization state and metallicity of the CGM by considering the relative abundances of different ions at low- and high-ionization states (e.g. Savage et al. 2002; Stocke et al. 2006). For example, attributing observed O\,VI absorbers to cool ($T \sim 10^4$ K), photoionized gas irradiated by the metagalactic ionizing radiation field, the observed column density ratios between O\,VI and low-ionization transitions (such as C\,III and C\,IV) require extremely low gas densities of $n_{\text{H}} \sim 10^{-5}\,\text{cm}^{-3}$. Combining the inferred low gas density with

observed $N(\text{O \textsc{vi}})$, which are typically $\gtrsim 10^{14.5}\,\text{cm}^{-2}$ in galactic haloes (e.g. Tumlinson et al. 2011), leads to a moderate gas metallicity of $\gtrsim 1/10$ Solar and unphysically large cloud sizes of $l_c \sim 1$ Mpc (e.g. Tripp et al. 2001; Savage et al. 2002; Stocke et al. 2006).[2] Excluding O \textsc{vi} due to possible origins in shocks or turbulent mixing layers (e.g. Heckman et al. 2002) and considering only relative abundances of low-ionization species increase estimated gas densities to $n_{\text{H}} \sim 10^{-4}$–$10^{-3}\,\text{cm}^{-3}$. The inferred cloud sizes remain large with $l_c \sim 10$–$100\,\text{kpc}$, in tension with what is observed locally for the HVCs. The implied thermal pressures in the cool gas phase are still two orders of magnitude lower than what is expected from pressure equilibrium with a hot ($T \approx 10^6$ K) medium (e.g. Stocke et al. 2013; Werk et al. 2014), indicating that these clouds would be crushed quickly. Considering non-equilibrium conditions (e.g. Gnat and Sternberg 2007; Oppenheimer and Schaye 2013) and the presence of local ionizing sources may help alleviate these problems (e.g. Cantalupo 2010), but the systematic uncertainties are difficult to quantify.

Nevertheless, exquisite details concerning extended halo gas have been learned over the past decade based on various samples of close galaxy and background QSO pairs. Because luminous QSOs are rare, roughly one QSO of $g \lesssim 18$ mag per square degree (e.g. Richards et al. 2006), absorption-line studies of the CGM against background QSO light have been largely limited to one probe per galaxy. Only in a few cases are multiple QSOs found at $d \lesssim 300\,\text{kpc}$ from a foreground galaxy (e.g. Norman et al. 1996; Keeney et al. 2013; Davis et al. 2015; Lehner et al. 2015; Bowen et al. 2016) for measuring coherence in spatial distribution and kinematics of extended gas around the galaxy. All of these cases are in the local Universe, because the relatively large angular extent of these galaxies on the sky increases the probability of finding more than one background QSO. This local sample has now been complemented with new studies, utilizing multiply lensed QSOs and close projected QSO pairs, which provide spatially resolved CGM absorption properties for a growing sample of galaxies at intermediate redshifts (e.g. Chen et al. 2014; Rubin et al. 2015; Zahedy et al. 2016).

With one QSO probe per halo, a two-dimensional map of CGM absorption properties can be established based on an ensemble average of a large sample of QSO-galaxy pairs ($N_{\text{pair}} \sim 100$–1000). Figure 9.6 summarizes some of the observable quantities of the CGM. First, panels (a) and (b) at the top display the radial profiles of rest-frame absorption equivalent width (W_r) for different absorption transitions, including hydrogen Lyα; low-ionization C \textsc{ii} and Si \textsc{ii}; intermediate-ionization Si \textsc{iii}, Si \textsc{iv} and C \textsc{iv}; and high-ionization O \textsc{vi} absorption transitions, colour-coded in black, red, orange, green, blue, magenta and dark purple, respectively. For transitions that are not detected, a 2-σ upper limit is shown as a downward arrow. Because of the large number of data points, the upper limits are shown in pale colours for

---

[2]For comparison, the sizes of extended HVC complexes at $d \sim 10\,\text{kpc}$ from the MW disk are a few to 15 kpc across (e.g. Putman et al. 2012). HVCs at larger distances are found to be more compact, $\lesssim 2\,\text{kpc}$ (e.g. Westmeier et al. 2008; Lockman et al. 2012; Giovanelli et al. 2013).
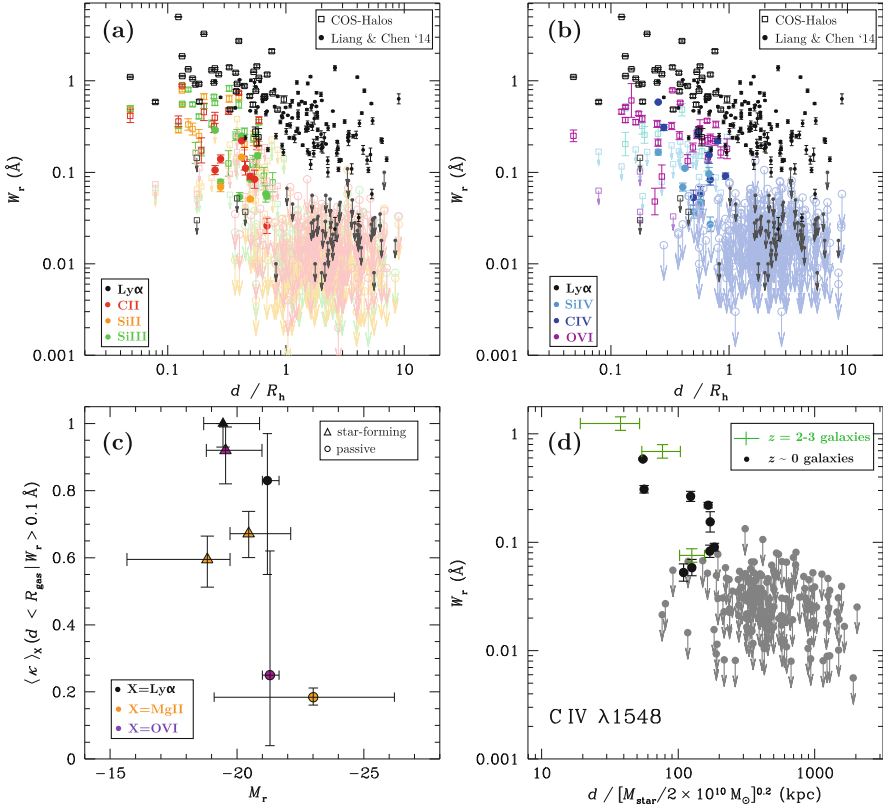
Fig. 9.6 Observed absorption properties of halo gas around galaxies. The *top panels* display the radial profiles of rest-frame absorption equivalent width (W_r) versus halo-radius R_h-normalized projected distance for different absorption transitions. Low-ionization transitions are presented in panel (**a**) and high-ionization transitions in panel (**b**). Lyα data points are presented in both panels for cross comparison. The galaxy sample includes 44 galaxies at $z \approx 0.25$ from the COS-Halos project (*open squares*; Tumlinson et al. 2011, 2013; Werk et al. 2013) and ∼200 galaxies at $z \approx$ 0.04 from public archives (*circles*; Liang and Chen 2014), for which high-quality, ultraviolet QSO spectra are available for constraining the presence or absence of multiple ions in individual haloes. Different transitions are colour-coded to highlight the differences in their spatial distributions. For transitions that are not detected, a 2-σ upper limit is shown by a *downward arrow*. No heavy ions are found beyond $d = R_h$, while Lyα continues to be seen to larger distances. Panel (**c**) displays the ensemble average of gas covering fraction ($\langle \kappa \rangle$) as a function of absolute r-band magnitude (M_r) for Lyα (*black symbols*), Mg II (*orange*) and O VI (*purple*). Star-forming galaxies (*triangles*) on average are fainter and exhibit higher covering fractions of hydrogen and chemically enriched gas probed by both low- and high-ionization species than passive galaxies (*circles*). Measurements of Lyα and O VI absorbing gas are based on COS-Halos galaxies for $R_{gas} = R_h$. Measurements of Mg II absorbing gas are based on ≈260 star-forming galaxies at $z \approx 0.25$ (Chen et al. 2010a) and ∼38,000 passive luminous red galaxies at $z \approx 0.5$ (Huang et al. 2016) for $R_{gas} = R_h/3$. Panel (**d**) illustrates the apparent constant nature of mass-normalized radial profiles of CGM absorption since $z \approx 3$ (e.g. Chen 2012; Liang and Chen 2014). The high-redshift observations are based on mean C IV absorption in stacked spectra of ∼500 starburst galaxies with a mean stellar mass and dispersion of $\langle \log M_{star} \rangle = 9.9 \pm 0.5$ (Steidel et al. 2010), and the low-redshift observations are for ∼200 individual galaxies with $\langle \log M_{star} \rangle = 9.7 \pm 1.1$ and modest SFR (Liang and Chen 2014)

clarity. The galaxy sample includes 44 galaxies at $z \approx 0.25$ from the COS-Halos project (open squares; Tumlinson et al. 2011, 2013; Werk et al. 2013) and $\sim$200 galaxies at $z \approx 0.04$ from public archives (circles; Liang and Chen 2014), for which high-quality, ultraviolet QSO spectra are available for constraining the presence or absence of multiple ions in individual haloes. These galaxies span four decades in total stellar mass, from $M_{\mathrm{star}} \approx 10^7\,M_\odot$ to $M_{\mathrm{star}} \approx 10^{11}\,M_\odot$, and a wide range in SFR, from SFR $< 0.1\,M_\odot\,\mathrm{yr}^{-1}$ to SFR $> 10\,M_\odot\,\mathrm{yr}^{-1}$. Diffuse gas is observed beyond $d = 50\,\mathrm{kpc}$ around distant galaxies, extending the detection limit of H I gas in inner galactic haloes from 21 cm observations (e.g. Fig. 9.2) to lower column density gas at larger distances and higher redshifts.

While W_{r} is typically found to decline steadily with increasing d for all transitions (e.g. Chen 2012; Werk et al. 2014), the scatters are large. Including the possibility that more massive haloes have more spatially extended halo gas, the halo radius R_{h}-normalized W_{r}-d distribution indeed displays substantially reduced scatters in the radial profiles shown in panels (a) and (b) of Fig. 9.6. A reduced scatter in the R_{h}-normalized W_{r}-d distribution indicates that galaxy mass plays a dominant role in driving the extent of halo gas. In addition, it also confirms that accurate associations between absorbers and absorbing galaxies have been found for the majority of the systems.

A particularly interesting feature in Fig. 9.6 is a complete absence of heavy ions beyond $d = R_{\mathrm{h}}$, while detections of Lyα continue to larger distances. The absence of heavy ions at $d > R_{\mathrm{h}}$, which is observed for a wide range of ionization states, strongly indicates that chemical enrichment is confined within individual galaxy haloes. This finding applies to both low-mass dwarfs and massive galaxies. However, it should also be noted that heavy ions are observed beyond R_{h} for galaxies with close neighbours (e.g. Borthakur et al. 2013; Johnson et al. 2015), suggesting that environmental effects play a role in distributing heavy elements beyond the enriched gaseous haloes of individual galaxies. Comparing panels (a) and (b) of Fig. 9.6 also shows that within individual galaxy haloes, a global ionization gradient is seen with more highly ionized gas detected at larger distances. For instance, the observed W_{r} declines to <0.1 Å at $d \approx 0.5\,R_{\mathrm{h}}$ for C II and Si II, while C IV and O VI absorbers of $W_{\mathrm{r}} > 0.1$ Å continue to be found beyond $0.5\,R_{\mathrm{h}}$.

The observed W_{r} versus d (or d/R_{h}) based on a blind survey of absorption features in the vicinities of known galaxies also enables measurements of gas covering fraction.[3] The mean gas covering fraction ($\langle \kappa \rangle$) can be measured by a simple accounting of the fraction of galaxies in an annular area displaying associated

---

[3]A blind survey of absorption features around known galaxies differs fundamentally from a blind survey of galaxies around known absorbers (e.g. Kacprzak et al. 2008). By design, a blind galaxy survey around known absorbers excludes transparent sightlines and does not provide the sample necessary for measuring the incidence and covering fraction of absorbing species. In addition, because of limited survey depths, a blind galaxy survey is more likely to find more luminous members at larger d that are correlated with the true absorbing galaxies which are fainter and closer to the QSO sightline, resulting in a significantly larger scatter in the W_{r} versus d distribution (e.g. Kacprzak et al. 2008; Nielsen et al. 2013).

absorbers with W_r exceeding some detection threshold W_0, and uncertainties can be estimated based on a binomial distribution function. Dividing the sample into different projected distance bins, it is clear from Fig. 9.6a, b that the fraction of non-detections increases with increasing projected distance, resulting in a declining $\langle \kappa \rangle$ with increasing d for all transitions observed (see also Chen et al. 2010a; Werk et al. 2014; Huang et al. 2016).

It is also interesting to examine how $\langle \kappa \rangle$ depends on galaxy properties. Figure 9.6c displays $\langle \kappa \rangle$ observed within a fiducial gaseous radius R_{gas} for star-forming (triangles) and passive (circles) galaxies. The measurements are made for Lyα (black symbols), Mg II (orange) and O VI (purple) with a threshold of $W_0 = 0.1$ Å and shown in relation to the absolute r-band magnitude (M_r). Error bars represent the 68% confidence interval. The absolute r-band magnitude is a direct observable of a galaxy and serves as a proxy for its underlying total stellar mass. Measurements of Lyα and O VI absorbing gas are based on COS-Halos galaxies for $R_{gas} = R_h$ (see also Johnson et al. (2015) for a sample compiled from the literature). Measurements of Mg II absorbing gas are based on ≈ 260 star-forming galaxies at $z \approx 0.25$ (Chen et al. 2010a) and $\sim 38{,}000$ passive luminous red galaxies at $z \approx 0.5$ (Huang et al. 2016) for $R_{gas} = R_h/3$ (e.g. Chen and Tinker 2008). The larger sample sizes led to better constrained $\langle \kappa \rangle$ for Mg II absorbing gas in galactic haloes. In general, star-forming galaxies on average are fainter and less massive and exhibit a higher covering fraction of chemically enriched gas than passive galaxies (see also Johnson et al. 2015). At the same time, the covering fraction of chemically enriched gas is definitely non-zero around massive quiescent galaxies.

Comparing the radial profiles of CGM absorption at different redshifts offers additional insights into the evolution history of the CGM, which in turn helps distinguish between different models for chemical enrichment in galaxy haloes. The radial profiles of the CGM have been found to evolve little since $z \sim 3$ (e.g. Chen 2012), even though the star-forming properties in galaxies have evolved significantly. Figure 9.6d illustrates the apparent constant nature of mass-normalized radial profiles of C IV absorption in galactic haloes (Liang and Chen 2014). The high-redshift observations are based on stacked spectra of ~ 500 starburst galaxies with a mean stellar mass and dispersion of $\langle \log M_{star} \rangle = 9.9 \pm 0.5$ (Steidel et al. 2010) and a mean SFR of $\langle SFR \rangle \approx 30\text{--}60 \, M_\odot \, \text{yr}^{-1}$ (e.g. Erb et al. 2006b; Reddy et al. 2012). The low-redshift galaxy sample contains individual measurements of ~ 200 galaxies with $\langle \log M_{star} \rangle = 9.7 \pm 1.1$ and more quiescent star-forming activities of $\langle SFR \rangle \sim 1 \, M_\odot \, \text{yr}^{-1}$ (Chen 2012; Liang and Chen 2014). The constant mass-normalized CGM radial profiles between galaxies of very different SFR indicate that mass (rather than SFR) is a dominant factor that determines the CGM properties over a cosmic time interval. This is consistent with previous findings that CGM absorption properties depend strongly on galaxy mass but only weakly on SFR (e.g. Chen et al. 2010b), but at odds with popular models that attribute metal-line absorbers to starburst-driven outflows (e.g. Steidel et al. 2010; Ménard et al. 2011).

A discriminating characteristic of starburst-driven outflows is their distinctly nonspherical distribution in galactic haloes in the presence of a well-formed star-forming disk. Specifically, galactic-scale outflows are expected to travel preferentially along the polar axis where the gas experiences the least resistance (e.g.

Heckman et al. 1990). In contrast, accretion of the IGM is expected to proceed along the disk plane with $\lesssim 10\%$ covering fraction on the sky (e.g. Faucher-Giguère and Kereš 2011; Fumagalli et al. 2011). Such azimuthal dependence of the spatial distribution of infalling and outflowing gas is fully realized in state-of-the-art cosmological zoom-in simulations (e.g. Shen et al. 2013; Agertz and Kravtsov 2015). Observations of $z \approx 0.7$ galaxies have shown that at $d < 50$ kpc, the mean Mg II absorption equivalent width within $45°$ of the minor axis is twice of the mean value found within $45°$ of the major axis, although such azimuthal dependence is not observed at $d > 50$ kpc (Bordoloi et al. 2011). The observed azimuthal dependence of the mean Mg II absorption strength is qualitatively consistent with the expectation that these heavy ions originate in starburst-driven outflows, and the lack of such azimuthal dependence implies that starburst outflows are confined to the inner halo of $d \lesssim 50$ kpc.

Many subsequent studies have generalized this observed azimuthal dependence at $d < 50$ kpc to larger distances and attributed absorbers detected near the minor axis to starburst-driven outflows and those found near the major axis to accretion (e.g. Bouché et al. 2012; Kacprzak et al. 2015). However, a causal connection between the observed absorbing gas and either outflows or accretion remains to be established. While gas metallicity may serve as a discriminator with the expectation of starburst outflows being more metal enriched relative to the low-density IGM, uncertainties arise due to poorly understood chemical mixing and metal transport (e.g. Tumlinson 2006). Incidentally, a relatively strong Mg II absorber has been found at $d \approx 60$ kpc along the minor axis of a starburst galaxy, but the metallicity of the absorbing gas is ten times lower than what is observed in the ISM (Kacprzak et al. 2014), highlighting the caveat of applying gas metallicity as the sole parameter for distinguishing between accretion and outflows.

Figure 9.7 presents visual comparisons of the geometric alignment of galaxy major axis relative to the QSO sightline and the observed CGM absorption strength. The figure at the top displays the observed O VI column density, $N(O\,VI)$, versus d for COS-Halos galaxies at $z \approx 0.2$ (Tumlinson et al. 2013). The bottom figure displays comparisons of $N(O\,VI)$ and $N(Mg\,II)$ for these galaxies. The absorption-line measurements are adopted from Werk et al. (2013). When spatially resolved images are available, the data points are replaced with an image panel of the absorbing galaxy. Each panel is 25 proper kpc on a side and is oriented such that the QSO sightline falls on the y-axis at the corresponding $N(O\,VI)$ of the galaxy. The relative alignment between galaxy major axis and the background QSO sightline cannot be determined, if the galaxies are face-on with a minor-to-major axis ratio > 0.7 or if the galaxies display irregular/asymmetric morphologies. These galaxies are labelled "F" and "A", respectively. For galaxies that clearly display a smooth and elongated morphology, the orientation of the major axis can be accurately measured. Galaxies with the QSO located within $30°$ of the minor axis are labelled "m", while galaxies with the QSO located within $30°$ of the major axis are labelled "M". Galaxies with the QSO sightline occuring intermediate (30–$60°$) between the minor and major axis are labelled "45". Star-forming galaxies are colour-coded in blue,
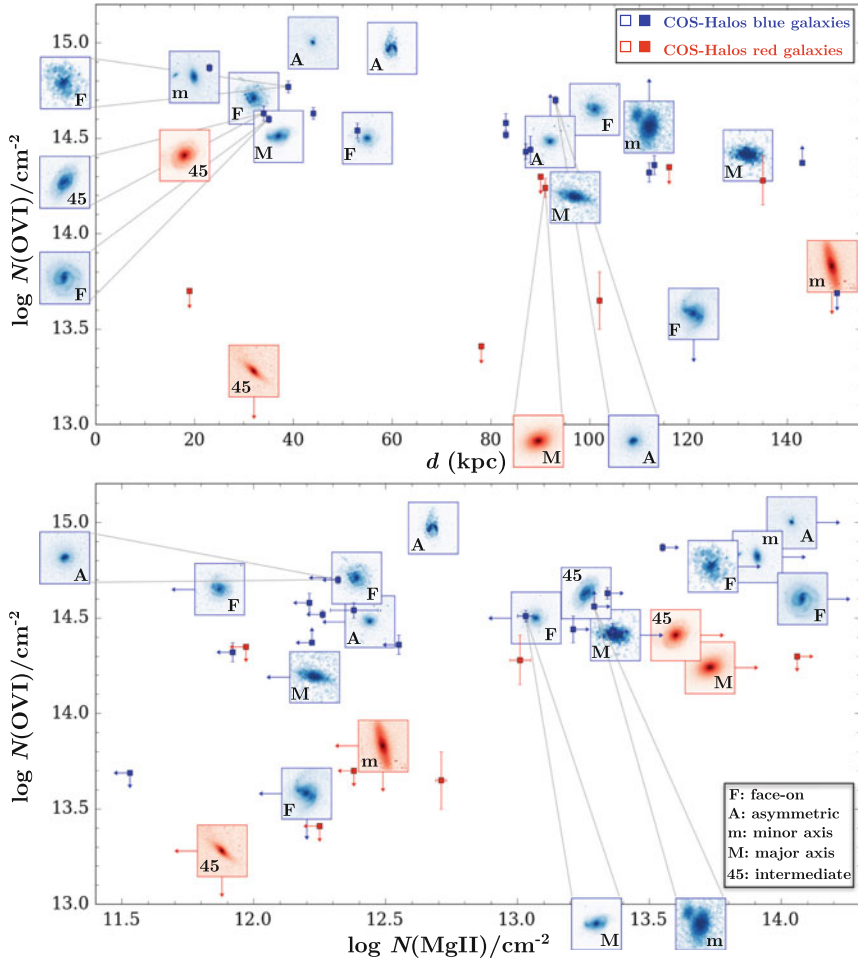
Fig. 9.7 Visual comparisons of the geometric alignment of galaxy major axis relative to the QSO sightline and the observed CGM absorption strength (by Rebecca Pierce). *Top*: observed O VI column density, N(O VI), versus d for COS-Halos star-forming (in *blue*) and passive (in *red*) galaxies (Tumlinson et al. 2011). *Bottom*: comparisons of N(O VI) and N(Mg II) for the COS-Halos galaxies from Werk et al. (2013). When spatially resolved images are available, the data points are replaced with an image panel of the absorbing galaxy. Each panel is 25 proper kpc on a side and is oriented such that the QSO sightline occurs on the *y*-axis at the corresponding O VI column density of the galaxy. Disk alignments cannot be determined for face-on galaxies (minor-to-major axis ratio > 0.7) and galaxies displaying irregular/asymmetric morphologies, which are labeled "F" and "A", respectively. Galaxies with the QSO located within 30° of the minor axis are labeled "m" in the lower-left corner, while galaxies with the QSO located within 30° of the major axis are labelled "M". Galaxies with the QSO sightline occurring intermediate (30–60°) between the minor and major axis are labelled "45". Downward arrows indicate 2-σ upper limits for non-detections, while upward arrows indicate saturated absorption lines. The COS-Halos galaxy sample provides a unique opportunity to examine low- and high-ionization halo gas for the same galaxies at once. Galaxies surrounded by O VI and Mg II absorbing gas clearly exhibit a broad range both in morphology and in disk orientation. In addition, the observed N(Mg II) displays a significantly larger scatter than N(O VI)

and passive galaxies in red. Downward arrows indicate 2-σ upper limits for non-detections, while upward arrows indicate saturated absorption lines.

While the COS-Halos sample is small, particularly when restricting to those galaxies displaying a smooth, elongated morphology, it provides a unique opportunity to examine low- and high-ionization halo gas for the same galaxies at once. Two interesting features are immediately clear in Fig. 9.7. First, galaxies surrounded by O VI and Mg II absorbing gas exhibit a broad range both in morphology and in star formation history, from compact quiescent galaxies to regular star-forming disks and to interacting pairs. The diverse morphologies in O VI and Mg II absorbing galaxies illuminate the challenge and uncertainties in characterizing their relative geometric orientation to the QSO sightline based on azimuthal angle alone. When considering only galaxies with smooth and elongated (minor-to-major axis ratio $<$ 0.7) morphologies, no clear dependence of N(O VI) or N(Mg II) on galaxy orientation is found. Specifically, nine star-forming galaxies displaying strong O VI absorption at $d <$ 80 kpc (log N(O VI)) have spatially resolved images available. Two of these galaxies display disturbed morphologies and four are nearly face-on. The remaining three galaxies have the inclined disks oriented at 0°, 45° and 90° each. For passive red galaxies, two have spatially resolved images available, and both are elongated and aligned at ≈45° from the QSO sightline. One displays an associated strong O VI absorber, and the other has no corresponding O VI detections. At $d >$ 80 kpc, the morphology distribution is similar to those at smaller distances. No strong dependence is found between the presence or absence of a strong O VI absorber and the galaxy orientation.

In addition, while the observed N(O VI) at $d <$ 100 kpc appears to be more uniformly distributed with a mean and scatter of log N(O VI) $= 14.5 \pm 0.3$ (Tumlinson et al. 2011), the observed N(Mg II) displays a significantly larger scatter. Specifically, the face-on galaxy at $d \approx$ 32 kpc with an associated O VI absorber of log N(O VI) $\approx$ 14.7 does not have an associated Mg II absorber detected to a limit of log N(Mg II) $\approx$ 12.4. Two quiescent galaxies at $z \approx$ 20 and 90 kpc (red panels) exhibit saturated Mg II absorption of log N(Mg II) $>$ 13.5 and similarly strong O VI of log N(O VI) $\approx$ 14.3. A small scatter implies a more uniformly distributed medium, while a large scatter implies a more clumpy nature of the absorbing gas or a larger variation between different galaxy haloes. Such distinct spatial distributions between low- and high-ionization gas further highlight the complex nature of the chemically enriched CGM, which depends on more than the geometric alignment of the galaxies. A three-dimensional model of gas kinematics that takes full advantage of the detailed morphologies and star formation history of the galaxies is expected to offer a deeper understanding of the physical origin of chemically enriched gas in galaxy haloes (e.g. Gauthier and Chen 2012; Chen et al. 2014; Diamond-Stanic et al. 2016).

9.6 Summary

QSO absorption spectroscopy provides a sensitive probe of both neutral medium and diffuse ionized gas in the distant Universe. It extends 21 cm maps of gaseous structures around low-redshift galaxies both to lower gas column densities and to higher redshifts. Specifically, DLAs of $N(\text{H\,I}) \gtrsim 2 \times 10^{20}\,\text{cm}^{-2}$ probe neutral gas in the ISM of distant star-forming galaxies, LLS of $N(\text{H\,I}) > 10^{17}\,\text{cm}^{-2}$ probe optically thick HVCs and gaseous streams in and around galaxies and strong Lyα absorbers of $N(\text{H\,I}) \approx 10^{14-17}\,\text{cm}^{-2}$ and associated metal-line absorption transitions, such as Mg\,II, C\,IV and O\,VI, trace chemically enriched, ionized gas and starburst outflows. Over the last decade, an unprecedentedly large number of $\sim$10,000 DLAs have been identified along random QSO sightlines to provide robust statistical characterizations of the incidence and mass density of neutral atomic gas at $z \lesssim 5$. Extensive follow-up studies have yielded accurate measurements of chemical compositions and molecular gas content for this neutral gas cross-section selected sample from $z \approx 5$ to $z \approx 0$ (Sect. 9.2). Combining galaxy surveys with absorption-line observations of gas around galaxies has enabled comprehensive studies of baryon cycles between star-forming regions and low-density gas over cosmic time. DLAs, while being rare as a result of a small cross-section of neutral medium in the Universe, have offered a unique window into gas dynamics and chemical enrichment in the outskirts of star-forming disks (Sect. 9.3), as well as star formation physics at high redshifts (Sect. 9.4). Observations of strong Lyα absorbers and associated ionic transitions around galaxies have also demonstrated that galaxy mass is a dominant factor in driving the extent of chemically enriched halo gas and that chemical enrichment is well confined within galactic haloes for both low-mass dwarfs and massive galaxies (Sect. 9.5).

With new observations carried out using new, multiplex instruments, continuing progress is expected in further advancing our understanding of baryonic cycles in the outskirts of galaxies over the next few years. These include, but are not limited to, (1) direct constraints for the star formation relation in different environments (e.g. Gnedin and Kravtsov 2010), particularly for star-forming galaxies at $z \gtrsim 2$ in low surface density regimes of $\Sigma_{\text{SFR}} < 0.1\,M_\odot\,\text{yr}^{-1}\,\text{kpc}^{-2}$ and $\Sigma_{\text{gas}} \approx 10\text{--}100\,M_\odot\,\text{pc}^{-2}$; (2) an empirical understanding of galaxy environmental effects in distributing heavy elements to large distances based on deep galaxy surveys carried out in a large number of QSO fields (e.g. Johnson et al. 2015); and (3) a three-dimensional map of gas flows in the circumgalactic space that combines absorption-line kinematics along multiple sightlines with optical morphologies of the absorbing galaxies and emission morphologies of extended gas around the galaxies (e.g. Rubin et al. 2011; Chen et al. 2014; Zahedy et al. 2016). Wide-field IFUs on existing large ground-based telescopes substantially increase the efficiency in faint galaxy surveys (e.g. Bacon et al. 2015) and in revealing extended low surface brightness emission features around high-redshift galaxies (e.g. Cantalupo et al. 2014; Borisova et al. 2016). The *James Webb Space Telescope* (*JWST*), which is scheduled to be launched in October 2018, will expand the sensitivity of detecting

faint star-forming galaxies in the early Universe. Combining deep infrared images from *JWST* and CO (or dust continuum) maps from ALMA will lead to critical constraints for the star formation relation in low surface density regimes.

References

Agertz, O., Kravtsov, A.V.: On the interplay between star formation and feedback in galaxy forma-tion simulations. Astrophys. J. **804**, 18 (2015). doi:10.1088/0004-637X/804/1/18, 1404.2613

Agertz, O., Teyssier, R., Moore, B.: Disc formation and the origin of clumpy galaxies at high red-shift. Mon. Not. R. Astron. Soc. **397**, L64–L68 (2009). doi:10.1111/j.1745-3933.2009.00685.x, 0901.2536

Aguirre, A., Dow-Hygelund, C., Schaye, J., Theuns, T.: Metallicity of the intergalactic medium using pixel statistics. IV. Oxygen. Astrophys. J. **689**, 851–864 (2008). doi:10.1086/592554, 0712.1239

Altay, G., Theuns, T., Schaye, J., Crighton, N.H.M., Dalla Vecchia, C.: Through thick and thin–H I absorption in cosmological simulations. Astrophys. J. Lett. **737**, L37 (2011). doi:10.1088/2041-8205/737/2/L37, 1012.4014

Altay, G., Theuns, T., Schaye, J., Booth, C.M., Dalla Vecchia, C.: The impact of different physical processes on the statistics of Lyman-limit and damped Lyman α absorbers. Mon. Not. R. Astron. Soc. **436**, 2689–2707 (2013). doi:10.1093/mnras/stt1765, 1307.6879

Bacon, R., Brinchmann, J., Richard, J., Contini, T., Drake, A., Franx, M., Tacchella, S., Vernet, J., Wisotzki, L., Blaizot, J., Bouché, N., Bouwens, R., Cantalupo, S., Carollo, C.M., Carton, D., Caruana, J., Clément, B., Dreizler, S., Epinat, B., Guiderdoni, B., Herenz, C., Husser, T.O., Kamann, S., Kerutt, J., Kollatschny, W., Krajnovic, D., Lilly, S., Martinsson, T., Michel-Dansac, L., Patricio, V., Schaye, J., Shirazi, M., Soto, K., Soucail, G., Steinmetz, M., Urrutia, T., Weilbacher, P., de Zeeuw, T.: The MUSE 3D view of the Hubble Deep Field South. Astron. Astrophys. **575**, A75 (2015). doi:10.1051/0004-6361/201425419, 1411.7667

Baker, A.J., Tacconi, L.J., Genzel, R., Lehnert, M.D., Lutz, D.: Molecular gas in the lensed Lyman break galaxy cB58. Astrophys. J. **604**, 125–140 (2004). doi:10.1086/381798, astro-ph/0312099

Balestra, I., Tozzi, P., Ettori, S., Rosati, P., Borgani, S., Mainieri, V., Norman, C., Viola, M.: Tracing the evolution in the iron content of the intra-cluster medium. Astron. Astrophys. **462**, 429–442 (2007). doi:10.1051/0004-6361:20065568, astro-ph/0609664

Beckwith, S.V.W., Stiavelli, M., Koekemoer, A.M., Caldwell, J.A.R., Ferguson, H.C., Hook, R., Lucas, R.A., Bergeron, L.E., Corbin, M., Jogee, S., Panagia, N., Robberto, M., Royle, P., Somerville, R.S., Sosey, M.: The Hubble ultra deep field. Astron. J. **132**, 1729–1755 (2006). doi:10.1086/507302, astro-ph/0607632

Bergeron, J., Boissé, P.: A sample of galaxies giving rise to Mg II quasar absorption systems. Astron. Astrophys. **243**, 344–366 (1991)

Bergeron, J., Stasińska, G.: Absorption line systems in QSO spectra - properties derived from observations and from photoionization models. Astron. Astrophys. **169**, 1–13 (1986)

Bigiel, F., Leroy, A., Walter, F., Brinks, E., de Blok, W.J.G., Madore, B., Thornley, M.D.: The star formation law in nearby galaxies on sub-Kpc scales. Astron. J. **136**, 2846–2871 (2008). doi:10.1088/0004-6256/136/6/2846, 0810.2541

Bigiel, F., Leroy, A., Walter, F., Blitz, L., Brinks, E., de Blok, W.J.G., Madore, B.: Extremely inefficient star formation in the outer disks of nearby galaxies. Astron. J. **140**, 1194–1213 (2010). doi:10.1088/0004-6256/140/5/1194, 1007.3498

Bird, S., Vogelsberger, M., Haehnelt, M., Sijacki, D., Genel, S., Torrey, P., Springel, V., Hernquist, L.: Damped Lyman α absorbers as a probe of stellar feedback. Mon. Not. R. Astron. Soc. **445**, 2313–2324 (2014). doi:10.1093/mnras/stu1923, 1405.3994

Boksenberg, A., Sargent, W.L.W.: Properties of QSO metal-line absorption systems at high redshifts: nature and evolution of the absorbers and new evidence on escape of ionizing radiation from galaxies. Astrophys. J. Suppl. Ser. **218**, 7 (2015). doi:10.1088/0067-0049/218/1/7, 1410.3784

Bordoloi, R., Lilly, S.J., Knobel, C., Bolzonella, M., Kampczyk, P., Carollo, C.M., Iovino, A., Zucca, E., Contini, T., Kneib, J.P., Le Fevre, O., Mainieri, V., Renzini, A., Scodeggio, M., Zamorani, G., Balestra, I., Bardelli, S., Bongiorno, A., Caputi, K., Cucciati, O., de la Torre, S., de Ravel, L., Garilli, B., Kovač, K., Lamareille, F., Le Borgne, J.F., Le Brun, V., Maier, C., Mignoli, M., Pello, R., Peng, Y., Perez Montero, E., Presotto, V., Scarlata, C., Silverman, J., Tanaka, M., Tasca, L., Tresse, L., Vergani, D., Barnes, L., Cappi, A., Cimatti, A., Coppa, G., Diener, C., Franzetti, P., Koekemoer, A., López-Sanjuan, C., McCracken, H.J., Moresco, M., Nair, P., Oesch, P., Pozzetti, L., Welikala, N.: The radial and azimuthal profiles of Mg II absorption around $0.5 < z < 0.9$ zCOSMOS Galaxies of different colors, masses, and environments. Astrophys. J. **743**, 10 (2011). doi:10.1088/0004-637X/743/1/10, 1106.0616

Borisova, E., Cantalupo, S., Lilly, S.J., Marino, R.A., Gallego, S.G., Bacon, R., Blaizot, J., Bouché, N., Brinchmann, J., Carollo, C.M., Caruana, J., Finley, H., Herenz, E.C., Richard, J., Schaye, J., Straka, L.A., Turner, M.L., Urrutia, T., Verhamme, A., Wisotzki, L.: Ubiquitous giant Ly α nebulae around the brightest quasars at $z \sim 3.5$ revealed with MUSE (2016). ArXiv e-prints 1605.01422

Borthakur, S., Heckman, T., Strickland, D., Wild, V., Schiminovich, D.: The impact of starbursts on the circumgalactic medium. Astrophys. J. **768**, 18 (2013). doi:10.1088/0004-637X/768/1/18, 1303.1183

Bouché, N., Hohensee, W., Vargas, R., Kacprzak, G.G., Martin, C.L., Cooke, J., Churchill, C.W. Physical properties of galactic winds using background quasars. Mon. Not. R. Astron. Soc. **426**, 801–815 (2012) doi:10.1111/j.1365-2966.2012.21114.x, 1110.5877

Bowen, D.V., Chelouche, D., Jenkins, E.B., Tripp, T.M., Pettini, M., York, D.G., Frye, B.L. The structure of the circumgalactic medium of galaxies: cool accretion inflow around NGC 1097. Astrophys. J. **826**, 50 (2016). doi:10.3847/0004-637X/826/1/50, 1605.04907

Braun, R.: Cosmological evolution of atomic gas and implications for 21 cm H I absorption. Astrophys. J. **749**, 87 (2012). doi:10.1088/0004-637X/749/1/87, 1202.1840

Bresolin, F., Kennicutt, R.C., Ryan-Weber, E.: Gas metallicities in the extended disks of NGC 1512 and NGC 3621. Chemical signatures of metal mixing or enriched gas accretion? Astrophys. J. **750**, 122 (2012). doi:10.1088/0004-637X/750/2/122, 1203.0956

Broeils, A.H., Rhee, M.H.: Short 21-cm WSRT observations of spiral and irregular galaxies. HI properties. Astron. Astrophys. **324**, 877–887 (1997)

Burbidge, E.M., Burbidge, G.R. Recent investigations of groups and clusters of galaxies. Astron. J. **66**, 541–550 (1961). doi:10.1086/108461

Cantalupo, S.: Stars quenching stars: how photoionization by local sources regulates gas cooling and galaxy formation. Mon. Not. R. Astron. Soc. **403**, L16–L20 (2010). doi:10.1111/j.1745-3933.2010.00806.x, 0912.4149

Cantalupo, S., Arrigoni-Battaia, F., Prochaska, J.X., Hennawi, J.F., Madau, P.: A cosmic web filament revealed in Lyman-α emission around a luminous high-redshift quasar. Nature **506**, 63–66 (2014). doi:10.1038/nature12898, 1401.4469

Cazaux, S., Spaans, M.: Molecular hydrogen formation on dust grains in the high-redshift universe. Astrophys. J. **611**, 40–51 (2004). doi:10.1086/422087, astro-ph/0404340

Chen, H.W.: The unchanging circumgalactic medium over the past 11 billion years. Mon. Not. R. Astron. Soc. **427**, 1238–1244 (2012). doi:10.1111/j.1365-2966.2012.22053.x, 1209.1094

Chen, H.W., Lanzetta, K.M.: The nature of damped Lyα absorbing galaxies at z <= 1: a photometric redshift survey of damped Lyα absorbers. Astrophys. J. **597**, 706–729 (2003). doi:10.1086/378635, astro-ph/0308190

Chen, H.W., Prochaska, J.X.: The origin of a chemically enriched Lyα absorption system at Z = 0.167. Astrophys. J. Lett. **543**, L9–L13 (2000). doi:10.1086/318179, astro-ph/0009001

Chen, H.W., Tinker, J.L.: The Baryon content of dark matter halos: empirical constraints from Mg II absorbers. Astrophys. J. **687**, 745–756 (2008). doi:10.1086/591927, 0801.2169

Chen, H.W., Kennicutt R.C. Jr., Rauch, M.: Abundance profiles and kinematics of damped Lyα absorbing galaxies at z < 0.651. Astrophys. J. **620**, 703–722 (2005). doi:10.1086/427088, astro-ph/0411006

Chen, H.W., Perley, D.A., Pollack, L.K., Prochaska, J.X., Bloom, J.S., Dessauges-Zavadsky, M., Pettini, M., Lopez, S., Dall'aglio, A., Becker, G.D.: High-redshift starbursting dwarf galaxies revealed by γ-ray burst afterglows. Astrophys. J. **691**, 152–174 (2009). doi:10.1088/0004-637X/691/1/152, 0809.2608

Chen, H.W., Helsby, J.E., Gauthier, J.R., Shectman, S.A., Thompson, I.B., Tinker, J.L.: An empirical characterization of extended cool gas around Galaxies using Mg II absorption features. Astrophys. J. **714**, 1521–1541 (2010a). doi:10.1088/0004-637X/714/2/1521, 1004.0705

Chen, H.W., Wild, V., Tinker, J.L., Gauthier, J.R., Helsby, J.E., Shectman, S.A., Thompson, I.B.: What determines the incidence and extent of Mg II absorbing gas around galaxies? Astrophys. J. Lett. **724**, L176–L182 (2010b). doi:10.1088/2041-8205/724/2/L176, 1011.0735

Chen, H.W., Gauthier, J.R., Sharon, K., Johnson, S.D., Nair, P., Liang, C.J.: Spatially resolved velocity maps of halo gas around two intermediate-redshift galaxies. Mon. Not. R. Astron. Soc. **438**, 1435–1450 (2014). doi:10.1093/mnras/stt2288, 1312.0016

Christensen, L., Wisotzki, L., Roth, M.M., Sánchez, S.F., Kelz, A., Jahnke, K.: An integral field spectroscopic survey for high redshift damped Lyman-α galaxies. Astron. Astrophys. **468**, 587–601 (2007). doi:10.1051/0004-6361:20066410, 0704.0654

Christensen, L., Møller, P., Fynbo, J.P.U., Zafar, T.: Verifying the mass-metallicity relation in damped Lyman α selected galaxies at 0.1 < z < 3.2. Mon. Not. R. Astron. Soc. **445**, 225–238 (2014). doi:10.1093/mnras/stu1726, 1404.6529

Chynoweth, K.M., Langston, G.I., Yun, M.S., Lockman, F.J., Rubin, K.H.R., Scoles, S.A.: Neutral hydrogen clouds in the M81/M82 group. Astron. J. **135**, 1983–1992 (2008). doi:10.1088/0004-6256/135/6/1983, 0803.3631

Cooke, J., Wolfe, A.M., Gawiser, E., Prochaska, J.X.: Survey for Galaxies associated with z ∼ 3 damped Lyα systems. II. Galaxy-absorber correlation functions. Astrophys. J. **652**, 994–1010 (2006). doi:10.1086/507476, astro-ph/0607149

Crighton, N.H.M., Murphy, M.T., Prochaska, J.X., Worseck, G., Rafelski, M., Becker, G.D., Ellison, S.L., Fumagalli, M., Lopez, S., Meiksin, A., O'Meara, J.M.: The neutral hydrogen cosmological mass density at z = 5. Mon. Not. R. Astron. Soc. **452**, 217–234 (2015). doi:10.1093/mnras/stv1182, 1506.02037

Davies, R., Förster Schreiber, N.M., Cresci, G., Genzel, R., Bouché, N., Burkert, A., Buschkamp, P., Genel, S., Hicks, E., Kurk, J., Lutz, D., Newman, S., Shapiro, K., Sternberg, A., Tacconi, L.J., Wuyts, S.: How well can we measure the intrinsic velocity dispersion of distant disk galaxies? Astrophys. J. **741**, 69 (2011). doi:10.1088/0004-637X/741/2/69, 1108.0285

Davis, J.D., Keeney, B.A., Danforth, C.W., Stocke, J.T.: On the size and mass of photoionized clouds in extended spiral galaxy halos. Astrophys. J. **810**, 92 (2015). doi:10.1088/0004-637X/810/2/92, 1506.04095

Decarli, R., Walter, F., Aravena, M., Carilli, C., Bouwens, R., da Cunha, E., Daddi, E., Ivison, R.J., Popping, G., Riechers, D., Smail, I., Swinbank, M., Weiss, A., Anguita, T., Assef, R., Bauer, F., Bell, E.F., Bertoldi, F., Chapman, S., Colina, L., Cortes, P.C., Cox, P., Dickinson, M., Elbaz, D., Gónzalez-López, J., Ibar, E., Infante, L., Hodge, J., Karim, A., Le Fevre, O., Magnelli, B., Neri, R., Oesch, P., Ota, K., Rix, H.W., Sargent, M., Sheth, K., van der Wel, A., van der Werf, P., Wagg, J.: ALMA spectroscopic survey in the Hubble Ultra Deep Field: CO luminosity functions and the evolution of the cosmic density of molecular gas (2016). arXiv e-prints 1607.06770

Dessauges-Zavadsky, M., D'Odorico, S., Schaerer, D., Modigliani, A., Tapken, C., Vernet, J.: Rest-frame ultraviolet spectrum of the gravitationally lensed galaxy "the 8 o'clock arc": stellar and interstellar medium properties. Astron. Astrophys. **510**, A26 (2010). doi:10.1051/0004-6361/200913337, 0912.4384

Diamond-Stanic, A.M., Coil, A.L., Moustakas, J., Tremonti, C.A., Sell, P.H., Mendez, A.J., Hickox, R.C., Rudnick, G.H.: Galaxies probing Galaxies at high resolution: co-rotating gas associated with a milky way analog at z = 0.4. Astrophys. J. **824**, 24 (2016). doi:10.3847/0004-637X/824/1/24, 1507.01945

D'Odorico, V., Cristiani, S., Pomante, E., Carswell, R.F., Viel, M., Barai, P., Becker, G.D., Calura, F., Cupani, G., Fontanot, F., Haehnelt, M.G., Kim, T.S., Miralda-Escudé, J., Rorai, A., Tescari, E., Vanzella, E.: Metals in the $z \sim 3$ intergalactic medium: results from an ultra-high signal-to-noise ratio UVES quasar spectrum. Mon. Not. R. Astron. Soc. (2016) doi:10.1093/mnras/stw2161, 1608.06116

Elmegreen, B.G.: A pressure and metallicity dependence for molecular cloud correlations and the calibration of mass. Astrophys. J. **338**, 178–196 (1989). doi:10.1086/167192

Elmegreen, B.G.: The H to H2 transition in galaxies - totally molecular galaxies. Astrophys. J. **411**, 170–177 (1993). doi:10.1086/172816

Erb, D.K., Shapley, A.E., Pettini, M., Steidel, C.C., Reddy, N.A., Adelberger, K.L.: The mass-metallicity relation at z> $\sim$ 2. Astrophys. J. **644**, 813–828 (2006a). doi:10.1086/503623, astro-ph/0602473

Erb, D.K., Steidel, C.C., Shapley, A.E., Pettini, M., Reddy, N.A., Adelberger, K.L.: Hα Observations of a large sample of galaxies at z $\sim$ 2: implications for star formation in high-redshift galaxies. Astrophys. J. **647**, 128–139 (2006b). doi:10.1086/505341, astro-ph/0604388

Erkal, D., Gnedin, N.Y., Kravtsov, A.V.: On the origin of the high column density turnover in the H I column density distribution. Astrophys. J. **761**, 54 (2012). doi:10.1088/0004-637X/761/1/54, 1201.3653

Faucher-Giguère, C.A., Kereš, D.: The small covering factor of cold accretion streams. Mon. Not. R. Astron. Soc. **412**, L118–L122 (2011). doi:10.1111/j.1745-3933.2011.01018.x, 1011.1693

Fernández, X., van Gorkom, J.H., Hess, K.M., Pisano, D.J., Kreckel, K., Momjian, E., Popping, A., Oosterloo, T., Chomiuk, L., Verheijen, M.A.W., Henning, P.A., Schiminovich, D., Bershady, M.A., Wilcots, E.M., Scoville, N.: A pilot for a very large array H I deep field. Astrophys. J. Lett. **770**, L29 (2013). doi:10.1088/2041-8205/770/2/L29, 1303.2659

Förster Schreiber, N.M., Genzel, R., Bouché, N., Cresci, G., Davies, R., Buschkamp, P., Shapiro, K., Tacconi, L.J., Hicks, E.K.S., Genel, S., Shapley, A.E., Erb, D.K., Steidel, C.C., Lutz, D., Eisenhauer, F., Gillessen, S., Sternberg, A., Renzini, A., Cimatti, A., Daddi, E., Kurk, J., Lilly, S., Kong, X., Lehnert, M.D., Nesvadba, N., Verma, A., McCracken, H., Arimoto, N., Mignoli, M., Onodera, M.: The SINS survey: SINFONI integral field spectroscopy of z $\sim$ 2 star-forming galaxies. Astrophys. J. **706**, 1364–1428 (2009). doi:10.1088/0004-637X/706/2/1364, 0903.1872

Friis, M., De Cia, A., Krühler, T., Fynbo, J.P.U., Ledoux, C., Vreeswijk, P.M., Watson, D.J., Malesani, D., Gorosabel, J., Starling, R.L.C., Jakobsson, P., Varela, K., Wiersema, K., Drachmann, A.P., Trotter, A., Thöne, C.C., de Ugarte Postigo, A., D'Elia, V., Elliott, J., Maturi, M., Goldoni, P., Greiner, J., Haislip, J., Kaper, L., Knust, F., LaCluyze, A., Milvang-Jensen, B., Reichart, D., Schulze, S., Sudilovsky, V., Tanvir, N., Vergani, S.D.: The warm, the excited, and the molecular gas: GRB 121024A shining through its star-forming galaxy. Mon. Not. R. Astron. Soc. **451**, 167–183 (2015). doi:10.1093/mnras/stv960, 1409.6315

Fumagalli, M., Prochaska, J.X., Kasen, D., Dekel, A., Ceverino, D., Primack, J.R.: Absorption-line systems in simulated galaxies fed by cold streams. Mon. Not. R. Astron. Soc. **418**, 1796–1821 (2011). doi:10.1111/j.1365-2966.2011.19599.x, 1103.2130

Fumagalli, M., O'Meara, J.M., Prochaska, J.X., Rafelski, M., Kanekar, N.: Directly imaging damped Ly α galaxies at z > 2 - III. The star formation rates of neutral gas reservoirs at $z \sim 2.7$. Mon. Not. R. Astron. Soc. **446**, 3178–3198 (2015). doi:10.1093/mnras/stu2325, 1409.2880

Gallazzi, A., Brinchmann, J., Charlot, S., White, S.D.M.: A census of metals and baryons in stars in the local Universe. Mon. Not. R. Astron. Soc. **383**, 1439–1458 (2008). doi:10.1111/j.1365-2966.2007.12632.x, 0708.0533

Gauthier, J.R., Chen, H.W.: Empirical constraints of supergalactic winds at $z \gtrsim 0.5$. Mon. Not. R. Astron. Soc. **424**, 1952–1962 (2012). doi:10.1111/j.1365-2966.2012.21327.x, 1205.4037

Genzel, R., Tacconi, L.J., Gracia-Carpio, J., Sternberg, A., Cooper, M.C., Shapiro, K., Bolatto, A., Bouché, N., Bournaud, F., Burkert, A., Combes, F., Comerford, J., Cox, P., Davis, M., Schreiber, N.M.F., Garcia-Burillo, S., Lutz, D., Naab, T., Neri, R., Omont, A., Shapley, A., Weiner, B.: A study of the gas-star formation relation over cosmic time. Mon. Not. R. Astron. Soc. **407**, 2091–2108 (2010). doi:10.1111/j.1365-2966.2010.16969.x, 1003.5180

Giovanelli, R., Haynes, M.P., Adams, E.A.K., Cannon, J.M., Rhode, K.L., Salzer, J.J., Skillman, E.D., Bernstein-Cooper, E.Z., McQuinn, K.B.W.: ALFALFA discovery of the nearby gas-rich dwarf galaxy Leo P. I. H I observations. Astron. J. **146**, 15 (2013). doi:10.1088/0004-6256/146/1/15, 1305.0272

Gnat, O., Sternberg, A.: Time-dependent ionization in radiatively cooling gas. Astrophys. J. Suppl. Ser. **168**, 213–230 (2007). doi:10.1086/509786, astro-ph/0608181

Gnedin, N.Y., Draine, B.T.: Line overlap and self-shielding of molecular hydrogen in Galaxies. Astrophys. J. **795**, 37 (2014). doi:10.1088/0004-637X/795/1/37, 1406.4129

Gnedin, N.Y., Kravtsov, A.V.: On the Kennicutt-Schmidt relation of low-metallicity high-redshift Galaxies. Astrophys. J. **714**, 287–295 (2010). doi:10.1088/0004-637X/714/1/287, 0912.3005

Gnedin, N.Y., Tassis, K., Kravtsov, A.V.: Modeling molecular hydrogen and star formation in cosmological simulations. Astrophys. J. **697**, 55–67 (2009). doi:10.1088/0004-637X/697/1/55, 0810.4148

Graciá-Carpio, J., García-Burillo, S., Planesas, P., Fuente, A., Usero, A.: Evidence of enhanced star formation efficiency in luminous and ultraluminous infrared galaxies. Astron. Astrophys. **479**, 703–717 (2008). doi:10.1051/0004-6361:20078223, 0712.0582

Heckman, T.M., Armus, L., Miley, G.K.: On the nature and implications of starburst-driven galactic superwinds. Astrophys. J. Suppl. Ser. **74**, 833–868 (1990). doi:10.1086/191522

Heckman, T.M., Norman, C.A., Strickland, D.K., Sembach, K.R.: On the physical origin of O VI absorption-line systems. Astrophys. J. **577**, 691–700 (2002). doi:10.1086/342232, astro-ph/0205556

Hopkins, A.M., Rao, S.M., Turnshek, D.A.: The star formation history of damped Lyα absorbers. Astrophys. J. **630**, 108–114 (2005). doi:10.1086/432046, astro-ph/0505418

Huang, Y.H., Chen, H.W., Johnson, S.D., Weiner, B.J.: Characterizing the chemically enriched circumgalactic medium of $\sim$ 38000 luminous red galaxies in SDSS DR12. Mon. Not. R. Astron. Soc. **455**, 1713–1727 (2016) . doi:10.1093/mnras/stv2327, 1510.01336

Johnson, S.D., Chen, H.W., Mulchaey, J.S.: On the possible environmental effect in distributing heavy elements beyond individual gaseous haloes. Mon. Not. R. Astron. Soc. **449**, 3263–3273 (2015). doi:10.1093/mnras/stv553, 1503.04199

Jorgenson, R.A., Wolfe, A.M.: Spatially resolved emission of a high-redshift DLA Galaxy with the Keck/OSIRIS IFU. Astrophys. J. **785**, 16 (2014). doi:10.1088/0004-637X/785/1/16, 1311.0045

Jorgenson, R.A., Murphy, M.T., Thompson, R., Carswell, R.F.: The Magellan uniform survey of damped Lyman α systems - II. Paucity of strong molecular hydrogen absorption. Mon. Not. R. Astron. Soc. **443**, 2783–2800 (2014). doi:10.1093/mnras/stu1314, 1407.1111

Kacprzak, G.G., Churchill, C.W., Steidel, C.C., Murphy, M.T.: Halo gas cross sections and covering fractions of Mg II absorption selected galaxies. Astron. J. **135**, 922–927 (2008). doi:10.1088/0004-6256/135/3/922, 0710.5765

Kacprzak, G.G., Murphy, M.T., Churchill, C.W.: Galaxy group at $z = 0.3$ associated with the damped Lyman α system towards quasar Q1127-145. Mon. Not. R. Astron. Soc. **406**, 445–459 (2010). doi:10.1111/j.1365-2966.2010.16667.x, 1003.3669

Kacprzak, G.G., Martin, C.L., Bouché, N., Churchill, C.W., Cooke, J., LeReun, A., Schroetter, I., Ho, S.H., Klimek, E.: New perspective on Galaxy outflows from the first detection of both intrinsic and traverse metal-line absorption. Astrophys. J. Lett. **792**, L12 (2014). doi:10.1088/2041-8205/792/1/L12, 1407.4126

Kacprzak, G.G., Muzahid, S., Churchill, C.W., Nielsen, N.M., Charlton, J.C.: The azimuthal dependence of outflows and accretion detected using O VI absorption. Astrophys. J. **815**, 22 (2015). doi:10.1088/0004-637X/815/1/22, 1511.03275

Karachentsev, I.D., Kashibadze, O.G.: Masses of the local group and of the M81 group estimated from distortions in the local velocity field. Astrophysics **49**, 3–18 (2006). doi:10.1007/s10511-006-0002-6

Keeney, B.A., Stocke, J.T., Rosenberg, J.L., Danforth, C.W., Ryan-Weber, E.V., Shull, J.M., Savage, B.D., Green, J.C.: HST/COS spectra of three QSOs that probe the circumgalactic medium of a single spiral galaxy: evidence for gas recycling and outflow. Astrophys. J. **765**, 27 (2013). doi:10.1088/0004-637X/765/1/27, 1301.4242

Kennicutt, R.C. Jr.: The global Schmidt law in star-forming Galaxies. Astrophys. J. **498**, 541–552 (1998). doi:10.1086/305588, astro-ph/9712213

Kereš, D., Katz, N., Fardal, M., Davé, R., Weinberg, D.H.: Galaxies in a simulated ΛCDM Universe - I. Cold mode and hot cores. Mon. Not. R. Astron. Soc. **395**, 160–179 (2009). doi:10.1111/j.1365-2966.2009.14541.x, 0809.1430

Kim, T.S., Partl, A.M., Carswell, R.F., Müller, V.: The evolution of H I and C IV quasar absorption line systems at $1.9 < z < 3.2$. Astron. Astrophys. **552**, A77 (2013). doi:10.1051/0004-6361/201220042, 1302.6622

Krogager, J.K., Fynbo, J.P.U., Møller, P., Ledoux, C., Noterdaeme, P., Christensen, L., Milvang-Jensen, B., Sparre, M.: On the sizes of $z \gtrsim 2$ damped Lyα absorbing galaxies. Mon. Not. R. Astron. Soc. **424**, L1–L5 (2012). doi:10.1111/j.1745-3933.2012.01272.x, 1204.2833

Krühler, T., Ledoux, C., Fynbo, J.P.U., Vreeswijk, P.M., Schmidl, S., Malesani, D., Christensen, L., De Cia, A., Hjorth, J., Jakobsson, P., Kann, D.A., Kaper, L., Vergani, S.D., Afonso, P.M.J., Covino, S., de Ugarte Postigo, A., D'Elia, V., Filgas, R., Goldoni, P., Greiner, J., Hartoog, O.E., Milvang-Jensen, B., Nardini, M., Piranomonte, S., Rossi, A., Sánchez-Ramírez, R., Schady, P., Schulze, S., Sudilovsky, V., Tanvir, N.R., Tagliaferri, G., Watson, D.J., Wiersema, K., Wijers, R.A.M.J., Xu, D.: Molecular hydrogen in the damped Lyman α system towards GRB 120815A at z = 2.36. Astron. Astrophys. **557**, A18 (2013). doi:10.1051/0004-6361/201321772, 1304.7003

Krumholz, M.R., McKee, C.F., Tumlinson, J.: The atomic-to-molecular transition in Galaxies. II: H I and H_2 column densities. Astrophys. J. **693**, 216–235 (2009). doi:10.1088/0004-637X/693/1/216, 0811.0004

Lanzetta, K.M., Wolfe, A.M., Turnshek, D.A., Lu, L., McMahon, R.G., Hazard, C.: A new spectroscopic survey for damped Ly-alpha absorption lines from high-redshift galaxies. Astrophys. J. Suppl. Ser. **77**, 1–57 (1991). doi:10.1086/191596

Lanzetta, K.M., Yahata, N., Pascarelle, S., Chen, H.W., Fernández-Soto, A.: The star formation rate intensity distribution function: implications for the cosmic star formation rate history of the universe. Astrophys. J. **570**, 492–501 (2002). doi:10.1086/339774, astro-ph/0111129

Law, D.R., Steidel, C.C., Erb, D.K., Larkin, J.E., Pettini, M., Shapley, A.E., Wright, S.A.: Integral field spectroscopy of high-redshift star-forming Galaxies with laser-guided adaptive optics: evidence for dispersion-dominated kinematics. Astrophys. J. **669**, 929–946 (2007). doi:10.1086/521786, 0707.3634

Law, D.R., Steidel, C.C., Shapley, A.E., Nagy, S.R., Reddy, N.A., Erb, D.K.: An HST/WFC3-IR morphological survey of Galaxies at z = 1.5-3.6. I. Survey description and morphological properties of star-forming Galaxies. Astrophys. J. **745**, 85 (2012). doi:10.1088/0004-637X/745/1/85, 1107.3137

Ledoux, C., Vreeswijk, P.M., Smette, A., Fox, A.J., Petitjean, P., Ellison, S.L., Fynbo, J.P.U., Savaglio, S.: Physical conditions in high-redshift GRB-DLA absorbers observed with VLT/UVES: implications for molecular hydrogen searches. Astron. Astrophys. **506**, 661–675 (2009). doi:10.1051/0004-6361/200811572, 0907.1057

Lehner, N., Howk, J.C., Wakker, B.P.: Evidence for a massive, extended circumgalactic medium around the andromeda Galaxy. Astrophys. J. **804**, 79 (2015). doi:10.1088/0004-637X/804/2/79, 1404.6540

Lehnert, M.D., Heckman, T.M., Weaver, K.A.: Very extended X-ray and Hα emission in M82: implications for the superwind phenomenon. Astrophys. J. **523**, 575–584 (1999). doi:10.1086/307762, astro-ph/9904227

Leroy, A.K., Walter, F., Brinks, E., Bigiel, F., de Blok, W.J.G., Madore, B., Thornley, M.D.: The star formation efficiency in nearby galaxies: measuring where gas forms stars effectively. Astron. J. **136**, 2782–2845 (2008). doi:10.1088/0004-6256/136/6/2782, 0810.2556

Leroy, A.K., Bolatto, A., Gordon, K., Sandstrom, K., Gratier, P., Rosolowsky, E., Engelbracht, C.W., Mizuno, N., Corbelli, E., Fukui, Y., Kawamura, A.: The CO-to-H_2 conversion factor from infrared dust emission across the local group. Astrophys. J. **737**, 12 (2011). doi:10.1088/0004-637X/737/1/12, 1102.4618

Liang, C.J., Chen, H.W.: Mining circumgalactic baryons in the low-redshift universe. Mon. Not. R. Astron. Soc. **445**, 2061–2081 (2014). doi:10.1093/mnras/stu1901, 1402.3602

Lockman, F.J., Free, N.L., Shields, J.C.: The neutral hydrogen bridge between M31 and M33. Astron. J. **144**, 52 (2012). doi:10.1088/0004-6256/144/2/52, 1205.5235

Lopez, S., D'Odorico, V., Ellison, S.L., Becker, G.D., Christensen, L., Cupani, G., Denney, K.D., Paris, I., Worseck, G., Berg, T.A.M., Cristiani, S., Dessauges-Zavadsky, M., Haehnelt, M., Hamann, F., Hennawi, J., Irsic, V., Kim, T.S., Lopez, P., Saust, R.L., Menard, B., Perrotta, S., Prochaska, J.X., Sanchez-Ramirez, R., Vestergaard, M., Viel, M., Wisotzki, L.: XQ-100: a legacy survey of one hundred $3.5 < z < 4.5$ quasars observed with VLT/XSHOOTER (2016) . ArXiv e-prints 1607.08776

Lu, L., Sargent, W.L.W., Barlow, T.A., Churchill, C.W., Vogt, S.S.: Abundances at high redshifts: the chemical enrichment history of damped Ly alpha Galaxies. Astrophys. J. Suppl. Ser. **107**, 475 (1996). doi:10.1086/192373, astro-ph/9606044

Madau, P., Dickinson, M.: Cosmic star-formation history. Ann. Rev. Astron. Astrophys. **52**, 415–486 (2014). doi:10.1146/annurev-astro-081811-125615, 1403.0007

Maiolino, R., Nagao, T., Grazian, A., Cocchia, F., Marconi, A., Mannucci, F., Cimatti, A., Pipino, A., Ballero, S., Calura, F., Chiappini, C., Fontana, A., Granato, G.L., Matteucci, F., Pastorini, G., Pentericci, L., Risaliti, G., Salvati, M., Silva, L.: AMAZE. I. The evolution of the mass-metallicity relation at $z > 3$. Astron. Astrophys. **488**, 463–479 (2008). doi:10.1051/0004-6361:200809678, 0806.2410

Mannucci, F., Cresci, G., Maiolino, R., Marconi, A., Pastorini, G., Pozzetti, L., Gnerucci, A., Risaliti, G., Schneider, R., Lehnert, M., Salvati, M.: LSD: Lyman-break galaxies Stellar populations and Dynamics - I. Mass, metallicity and gas at $z \sim 3.1$. Mon. Not. R. Astron. Soc. **398**, 1915–1931 (2009). doi:10.1111/j.1365-2966.2009.15185.x, 0902.2398

Marasco, A., Crain, R.A., Schaye, J., Bahé, Y.M., van der Hulst, T., Theuns, T., Bower, R.G.: The environmental dependence of H I in galaxies in the EAGLE simulations. Mon. Not. R. Astron. Soc. **461**, 2630–2649 (2016). doi:10.1093/mnras/stw1498, 1606.06288

Martin, C.L., Kennicutt, R.C. Jr.: Star formation thresholds in galactic disks. Astrophys. J. **555**, 301–321 (2001). doi:10.1086/321452, astro-ph/0103181

McGaugh, S.S.: Oxygen abundances in low surface brightness disk galaxies. Astrophys. J. **426**, 135–149 (1994). doi:10.1086/174049, astro-ph/9311064

Ménard, B., Wild, V., Nestor, D., Quider, A., Zibetti, S., Rao, S., Turnshek, D.: Probing star formation across cosmic time with absorption-line systems. Mon. Not. R. Astron. Soc. **417**, 801–811 (2011). doi:10.1111/j.1365-2966.2011.18227.x, 0912.3263

Meyer, D.M., Welty, D.E., York, D.G.: Element abundances at high redshift. Astrophys. J. Lett. **343**, L37–L40 (1989). doi:10.1086/185505

Møller, P., Warren, S.J., Fall, S.M., Fynbo, J.U., Jakobsen, P.: Are high-redshift damped Lyα galaxies Lyman break galaxies? Astrophys. J. **574**, 51–58 (2002). doi:10.1086/340934, astro-ph/0203361

Møller, P., Fynbo, J.P.U., Fall, S.M.: Detection of Lyman-α emission from a DLA galaxy: possible implications for a luminosity-metallicity relation at $z = 2$-3. Astron. Astrophys. **422**, L33–L37 (2004). doi:10.1051/0004-6361:20040194, astro-ph/0406307

Muzahid, S., Srianand, R., Charlton, J.: An HST/COS survey of molecular hydrogen in DLAs & sub-DLAs at z < 1: molecular fraction and excitation temperature. Mon. Not. R. Astron. Soc. **448**, 2840–2853 (2015). doi:10.1093/mnras/stv133, 1410.3828

Neeleman, M., Wolfe, A.M., Prochaska, J.X., Rafelski, M.: The fundamental plane of damped Lyα systems. Astrophys. J. **769**, 54 (2013). doi:10.1088/0004-637X/769/1/54, 1303.7239

Neeleman, M., Prochaska, J.X., Ribaudo, J., Lehner, N., Howk, J.C., Rafelski, M., Kanekar, N.: The H I content of the universe over the past 10 Gyrs. Astrophys. J. **818**, 113 (2016a). doi:10.3847/0004-637X/818/2/113, 1601.01691

Neeleman, M., Prochaska, J.X., Zwaan, M.A., Kanekar, N., Christensen, L., Dessauges-Zavadsky, M., Fynbo, J.P.U., van Kampen, E., Møller, P., Zafar, T.: First connection between cold gas in emission and absorption: CO emission from a Galaxy-Quasar pair. Astrophys. J. Lett. **820**, L39 (2016b). doi:10.3847/2041-8205/820/2/L39, 1604.05720

Nielsen, N.M., Churchill, C.W., Kacprzak, G.G.: MAGIICAT II. general characteristics of the Mg II absorbing circumgalactic medium. Astrophys. J. **776**, 115 (2013). doi:10.1088/0004-637X/776/2/115, 1211.1380

Norman, C.A., Bowen, D.V., Heckman, T., Blades, C., Danly, L.: Hubble space telescope observations of QSO absorption lines associated with starburst galaxy outflows. Astrophys. J. **472**, 73 (1996). doi:10.1086/178042

Noterdaeme, P., Ledoux, C., Petitjean, P., Srianand, R.: Molecular hydrogen in high-redshift damped Lyman-α systems: the VLT/UVES database. Astron. Astrophys. **481**, 327–336 (2008). doi:10.1051/0004-6361:20078780, 0801.3682

Noterdaeme, P., Petitjean, P., Ledoux, C., Srianand, R.: Evolution of the cosmological mass density of neutral gas from Sloan Digital Sky Survey II - Data Release 7. Astron. Astrophys. **505**, 1087–1098 (2009). doi:10.1051/0004-6361/200912768, 0908.1574

Noterdaeme, P., Petitjean, P., Carithers, W.C., Pâris, I., Font-Ribera, A., Bailey, S., Aubourg, E., Bizyaev, D., Ebelke, G., Finley, H., Ge, J., Malanushenko, E., Malanushenko, V., Miralda-Escudé, J., Myers, A.D., Oravetz, D., Pan, K., Pieri, M.M., Ross, N.P., Schneider, D.P., Simmons, A., York, D.G.: Column density distribution and cosmological mass density of neutral gas: Sloan Digital Sky Survey-III Data Release 9. Astron. Astrophys. **547**, L1 (2012). doi:10.1051/0004-6361/201220259, 1210.1213

Noterdaeme, P., Petitjean, P., Srianand, R.: The elusive HI→H$_2$ transition in high-z damped Lyman-α systems. Astron. Astrophys. **578**, L5 (2015). doi:10.1051/0004-6361/201526018, 1505.04997

Noterdaeme, P., Krogager, J.K., Balashev, S., Ge, J., Gupta, N., Krühler, T., Ledoux, C., Murphy, M.T., Pâris, I., Petitjean, P., Rahmani, H., Srianand, R., Ubachs, W.: Discovery of a Perseus-like cloud in the early Universe: HI-to-H2 transition, carbon monoxide and small dust grains at zabs=2.53 towards the quasar J0000+0048 (2016) . ArXiv e-prints 1609.01422

Oosterloo, T., Morganti, R., Crocker, A., Jütte, E., Cappellari, M., de Zeeuw, T., Krajnović, D., McDermid, R., Kuntschner, H., Sarzi, M., Weijmans, A.M.: Early-type galaxies in different environments: an HI view. Mon. Not. R. Astron. Soc. **409**, 500–514 (2010). doi:10.1111/j.1365-2966.2010.17351.x, 1007.2059

Oppenheimer, B.D., Schaye, J.: Non-equilibrium ionization and cooling of metal-enriched gas in the presence of a photoionization background. Mon. Not. R. Astron. Soc. **434**, 1043–1062 (2013). doi:10.1093/mnras/stt1043, 1302.5710

Péroux, C., Bouché, N., Kulkarni, V.P., York, D.G., Vladilo, G.: A SINFONI integral field spectroscopy survey for galaxy counterparts to damped Lyman α systems - I. New detections and limits for intervening and associated absorbers. Mon. Not. R. Astron. Soc. **410**, 2237–2250 (2011). doi:10.1111/j.1365-2966.2010.17598.x, 1009.0025

Péroux, C., Bouché, N., Kulkarni, V.P., York, D.G., Vladilo, G.: A SINFONI integral field spectroscopy survey for galaxy counterparts to damped Lyman α systems - III. Three additional detections. Mon. Not. R. Astron. Soc. **419**, 3060–3073 (2012). doi:10.1111/j.1365-2966.2011.19947.x, 1110.0666

Péroux, C., Quiret, S., Rahmani, H., Kulkarni, V.P., Epinat, B., Milliard, B., Straka, L.A., York, D.G., Rahmati, A., Contini, T.: A SINFONI integral field spectroscopy survey for galaxy

counterparts to damped Lyman α systems - VI. Metallicity and geometry as gas flow probes. Mon. Not. R. Astron. Soc. **457**, 903–916 (2016). doi:10.1093/mnras/stw016, 1601.02796

Pettini, M.: Element abundances through the cosmic ages. In: Esteban, C., García López, R., Herrero, A., Sánchez, F. (eds.) Cosmochemistry. The Melting Pot of the Elements, pp. 257–298 (2004). astro-ph/0303272

Pettini, M., Boksenberg, A., Hunstead, R.W.: Metal enrichment, dust, and star formation in galaxies at high redshifts. I - The Z = 2.3091 absorber toward PHL 957. Astrophys. J. **348**, 48–56 (1990). doi:10.1086/168212

Pettini, M., Ellison, S.L., Steidel, C.C., Bowen, D.V.: Metal abundances at z<1.5: fresh clues to the chemical enrichment history of damped Lyα systems. Astrophys. J. **510**, 576–589 (1999). doi:10.1086/306635, astro-ph/9808017

Pettini, M., Shapley, A.E., Steidel, C.C., Cuby, J.G., Dickinson, M., Moorwood, A.F.M., Adelberger, K.L., Giavalisco, M.: The rest-frame optical spectra of Lyman break galaxies: star formation, extinction, abundances, and kinematics. Astrophys. J. **554**, 981–1000 (2001). doi:10.1086/321403, astro-ph/0102456

Pettini, M., Rix, S.A., Steidel, C.C., Adelberger, K.L., Hunt, M.P., Shapley, A.E.: New observations of the interstellar medium in the Lyman break galaxy MS 1512-cB58. Astrophys. J. **569**, 742–757 (2002). doi:10.1086/339355, astro-ph/0110637

Prochaska, J.X., Tumlinson, J.: Baryons: what, when and where? Astrophys. Space Sci. Proc. **10**, 419 (2009). doi:10.1007/978-1-4020-9457-6_16, 0805.4635

Prochaska, J.X., Wolfe, A.M.: A Keck HIRES investigation of the metal abundances and kinematics of the Z = 2.46 damped LY alpha system toward Q0201+365. Astrophys. J. **470**, 403 (1996). doi:10.1086/177875, astro-ph/9604042

Prochaska, J.X., Wolfe, A.M.: Chemical abundances of the damped Lyα systems at z>1.5. Astrophys. J. Suppl. Ser. **121**, 369–415 (1999). doi:10.1086/313200, astro-ph/9810381

Prochaska, J.X., Wolfe, A.M.: On the (Non)evolution of H I gas in galaxies over cosmic time. Astrophys. J. **696**, 1543–1547 (2009). doi:10.1088/0004-637X/696/2/1543, 0811.2003

Prochaska, J.X., Howk, J.C., O'Meara, J.M., Tytler, D., Wolfe, A.M., Kirkman, D., Lubin, D., Suzuki, N.: The UCSD HIRES/Keck I damped Lyα abundance database. III. An empirical study of photoionization in the damped Lyα system toward GB 1759+7539. Astrophys. J. **571**, 693–711 (2002). doi:10.1086/340066, astro-ph/0202140

Prochaska, J.X., Sheffer, Y., Perley, D.A., Bloom, J.S., Lopez, L.A., Dessauges-Zavadsky, M., Chen, H.W., Filippenko, A.V., Ganeshalingam, M., Li, W., Miller, A.A., Starr, D.: The first positive detection of molecular gas in a GRB host galaxy. Astrophys. J. Lett. **691**, L27–L32 (2009). doi:10.1088/0004-637X/691/1/L27, 0901.0556

Putman, M.E., Peek, J.E.G., Joung, M.R.: Gaseous galaxy halos. Ann. Rev. Astron. Astrophys. **50**, 491–529 (2012). doi:10.1146/annurev-astro-081811-125612, 1207.4837

Rafelski, M., Wolfe, A.M., Chen, H.W.: Star formation from DLA gas in the outskirts of Lyman break galaxies at z $\sim$ 3. Astrophys. J. **736**, 48 (2011). doi:10.1088/0004-637X/736/1/48, 1011.6390

Rafelski, M., Wolfe, A.M., Prochaska, J.X., Neeleman, M., Mendez, A.J.: Metallicity evolution of damped Lyα systems out to z $\sim$ 5. Astrophys. J. **755**, 89 (2012). doi:10.1088/0004-637X/755/2/89, 1205.5047

Rafelski, M., Neeleman, M., Fumagalli, M., Wolfe, A.M., Prochaska, J.X.: The rapid decline in metallicity of damped Lyα systems at z $\sim$ 5. Astrophys. J. Lett. **782**, L29 (2014). doi:10.1088/2041-8205/782/2/L29, 1310.6042

Rafelski, M., Gardner, J.P., Fumagalli, M., Neeleman, M., Teplitz, H.I., Grogin, N., Koekemoer, A.M., Scarlata, C.: The star formation rate efficiency of neutral atomic-dominated hydrogen gas in the outskirts of star-forming galaxies from z $\sim$ 1 to z $\sim$ 3. Astrophys. J. **825**, 87 (2016). doi:10.3847/0004-637X/825/2/87, 1604.08597

Rao, S.M., Nestor, D.B., Turnshek, D.A., Lane, W.M., Monier, E.M., Bergeron, J.: Low-redshift damped Lyα galaxies toward the Quasars B2 0827+243, PKS 0952+179, PKS 1127-145, and PKS 1629+120. Astrophys. J. **595**, 94–108 (2003). doi:10.1086/377331, astro-ph/0211297

Rao, S.M., Turnshek, D.A., Nestor, D.B.: Damped Lyα systems at z<1.65: the expanded Sloan Digital Sky Survey hubble space telescope sample. Astrophys. J. **636**, 610–630 (2006). doi:10.1086/498132, astro-ph/0509469

Rao, S.M., Belfort-Mihalyi, M., Turnshek, D.A., Monier, E.M., Nestor, D.B., Quider, A.: A ground-based imaging study of galaxies causing damped Lyman α (DLA), sub-DLA and Lyman limit system absorption in quasar spectra. Mon. Not. R. Astron. Soc. **416**, 1215–1249 (2011). doi:10.1111/j.1365-2966.2011.19119.x, 1103.4047

Rauch, M.: The Lyman alpha forest in the spectra of QSOs. Ann. Rev. Astron. Astrophys. **36**, 267–316 (1998). doi:10.1146/annurev.astro.36.1.267, astro-ph/9806286

Rauch, M., Sargent, W.L.W., Womble, D.S., Barlow, T.A.: Temperature and kinematics of C IV absorption systems. Astrophys. J. Lett. **467**, L5 (1996). doi:10.1086/310187, astro-ph/9606041

Reddy, N.A., Pettini, M., Steidel, C.C., Shapley, A.E., Erb, D.K., Law, D.R.: The characteristic star formation histories of galaxies at redshifts z∼2-7. Astrophys. J. **754**, 25 (2012). doi:10.1088/0004-637X/754/1/25, 1205.0555

Rémy-Ruyer, A., Madden, S.C., Galliano, F., Galametz, M., Takeuchi, T.T., Asano, R.S., Zhukovska, S., Lebouteiller, V., Cormier, D., Jones, A., Bocchio, M., Baes, M., Bendo, G.J., Boquien, M., Boselli, A., DeLooze, I., Doublier-Pritchard, V., Hughes, T., Karczewski, O.Ł., Spinoglio, L.: Gas-to-dust mass ratios in local galaxies over a 2 dex metallicity range. Astron. Astrophys. **563**, A31 (2014). doi:10.1051/0004-6361/201322803, 1312.3442

Richards, G.T., Strauss, M.A., Fan, X., Hall, P.B., Jester, S., Schneider, D.P., Vanden Berk, D.E., Stoughton, C., Anderson, S.F., Brunner, R.J., Gray, J., Gunn, J.E., Ivezić, Ž., Kirkland, M.K., Knapp, G.R., Loveday, J., Meiksin, A., Pope, A., Szalay, A.S., Thakar, A.R., Yanny, B., York, D.G., Barentine, J.C., Brewington, H.J., Brinkmann, J., Fukugita, M., Harvanek, M., Kent, S.M., Kleinman, S.J., Krzesiński, J., Long, D.C., Lupton, R.H., Nash T., Neilsen, E.H. Jr., Nitta, A., Schlegel, D.J., Snedden, S.A.: The sloan digital sky survey Quasar survey: Quasar luminosity function from data release 3. Astron. J. **131**, 2766–2787 (2006). doi:10.1086/503559, astro-ph/0601434

Rigby, J.R., Charlton, J.C., Churchill, C.W.: The population of weak Mg II absorbers. II. The properties of single-cloud systems. Astrophys. J. **565**, 743–761 (2002). doi:10.1086/324723, astro-ph/0110191

Rubin, K.H.R., Prochaska, J.X., Ménard, B., Murray, N., Kasen, D., Koo, D.C., Phillips, A.C.: Low-ionization line emission from a starburst galaxy: a new probe of a galactic-scale outflow. Astrophys. J. **728**, 55 (2011). doi:10.1088/0004-637X/728/1/55, 1008.3397

Rubin, K.H.R., Hennawi, J.F., Prochaska, J.X., Simcoe, R.A., Myers, A., Lau, M.W.: (2015). Dissecting the gaseous halos of z∼2 damped Lyα systems with close Quasar pairs. Astrophys. J. **808**, 38. doi:10.1088/0004-637X/808/1/38, 1411.6016

Salim, S., Rich, R.M.: Star formation signatures in optically quiescent early-type galaxies. Astrophys. J. Lett. **714**, L290–L294 (2010). doi:10.1088/2041-8205/714/2/L290, 1004.2041

Sánchez, S.F., Rosales-Ortega, F.F., Iglesias-Páramo, J., Mollá, M., Barrera-Ballesteros, J., Marino, R.A., Pérez, E., Sánchez-Blazquez, P., González Delgado, R., Cid Fernandes, R., de Lorenzo-Cáceres, A., Mendez-Abreu, J., Galbany, L., Falcon-Barroso, J., Miralles-Caballero, D., Husemann, B., García-Benito, R., Mast, D., Walcher, C.J., Gil de Paz, A., García-Lorenzo, B., Jungwiert, B., Vílchez, J.M., Jílková, L., Lyubenova, M., Cortijo-Ferrero, C., Díaz, A.I., Wisotzki, L., Márquez, I., Bland-Hawthorn, J., Ellis, S., van de Ven, G., Jahnke, K., Papaderos, P., Gomes, J.M., Mendoza, M.A., López-Sánchez, Á.R.: A characteristic oxygen abundance gradient in galaxy disks unveiled with CALIFA. Astron. Astrophys. **563**, A49 (2014). doi:10.1051/0004-6361/201322343, 1311.7052

Sánchez-Ramírez, R., Ellison, S.L., Prochaska, J.X., Berg, T.A.M., López, S., D'Odorico, V., Becker, G.D., Christensen, L., Cupani, G., Denney, K.D., Pâris, I., Worseck, G., Gorosabel, J.: The evolution of neutral gas in damped Lyman α systems from the XQ-100 survey. Mon. Not. R. Astron. Soc. **456**, 4488–4505 (2016). doi:10.1093/mnras/stv2732, 1511.05003

Savage, B.D., Sembach, K.R.: Interstellar abundances from absorption-line observations with the hubble space telescope. Ann. Rev. Astron. Astrophys. **34**, 279–330 (1996). doi:10.1146/annurev.astro.34.1.279

Savage, B.D., Sembach, K.R., Tripp, T.M., Richter, P.: Far ultraviolet spectroscopic explorer and space telescope imaging spectrograph observations of intervening O VI absorption line systems in the spectrum of PG 0953+415. Astrophys. J. **564**, 631–649 (2002). doi:10.1086/324288

Schechter, P.: An analytic expression for the luminosity function for galaxies. Astrophys. J. **203**, 297–306 (1976). doi:10.1086/154079

Schmidt, M.: The rate of star formation. Astrophys. J. **129**, 243 (1959). doi:10.1086/146614

Serra, P., Oosterloo, T., Morganti, R., Alatalo, K., Blitz, L., Bois, M., Bournaud, F., Bureau, M., Cappellari, M., Crocker, A.F., Davies, R.L., Davis, T.A., de Zeeuw, P.T., Duc, P.A., Emsellem, E., Khochfar, S., Krajnović, D., Kuntschner, H., Lablanche, P.Y., McDermid, R.M., Naab, T., Sarzi, M., Scott, N., Trager, S.C., Weijmans, A.M., Young, L.M.: The ATLAS^{3D} project - XIII. Mass and morphology of H I in early-type galaxies as a function of environment. Mon. Not. R. Astron. Soc. **422**, 1835–1862 (2012). doi:10.1111/j.1365-2966.2012.20219.x, 1111.4241

Shen, S., Madau, P., Guedes, J., Mayer, L., Prochaska, J.X., Wadsley, J.: The circumgalactic medium of massive galaxies at z ∼ 3: a test for stellar feedback, galactic outflows, and cold streams. Astrophys. J. **765**, 89 (2013). DOI 10.1088/0004-637X/765/2/89, 1205.0270

Simcoe, R.A.: The carbon content of intergalactic gas at z = 4.25 and its evolution toward z = 2.4. Astrophys. J. **738**, 159 (2011). doi:10.1088/0004-637X/738/2/159, 1106.2810

Som, D., Kulkarni, V.P., Meiring, J., York, D.G., Péroux, C., Lauroesch, J.T., Aller, M.C., Khare, P.: Hubble space telescope observations of sub-damped Lyα absorbers at z < 0.5, and implications for galaxy chemical evolution. Astrophys. J. **806**, 25 (2015). doi:10.1088/0004-637X/806/1/25, 1502.01989

Steidel, C.C., Kollmeier, J.A., Shapley, A.E., Churchill, C.W., Dickinson, M., Pettini, M.: The kinematic connection between absorbing gas toward QSOs and galaxies at intermediate redshift. Astrophys. J. **570**, 526–542 (2002). doi:10.1086/339792, astro-ph/0201353

Steidel, C.C., Erb, D.K., Shapley, A.E., Pettini, M., Reddy, N., Bogosavljević, M., Rudie, G.C., Rakic, O.: The structure and kinematics of the circumgalactic medium from far-ultraviolet spectra of z ∼ = 2-3 galaxies. Astrophys. J. **717**, 289–322 (2010). doi:10.1088/0004-637X/717/1/289, 1003.0679

Stocke, J.T., Penton, S.V., Danforth, C.W., Shull, J.M., Tumlinson, J., McLin, K.M.: The galaxy environment of O VI absorption systems. Astrophys. J. **641**, 217–228 (2006). doi:10.1086/500386, astro-ph/0509822

Stocke, J.T., Keeney, B.A., Danforth, C.W., Shull, J.M., Froning, C.S., Green, J.C., Penton, S.V., Savage, B.D.: Characterizing the circumgalactic medium of nearby galaxies with HST/COS and HST/STIS absorption-line spectroscopy. Astrophys. J. **763**, 148 (2013). doi:10.1088/0004-637X/763/2/148, 1212.5658

Straka, L.A., Noterdaeme, P., Srianand, R., Nutalaya, S., Kulkarni, V.P., Khare, P., Bowen, D., Bishof, M., York, D.G.: Galactic nebular lines in the fibre spectra of background QSOs: reaching a hundred QSO-galaxy pairs with spectroscopic and photometric measurements. Mon. Not. R. Astron. Soc. **447**, 3856–3872 (2015). doi:10.1093/mnras/stu2739, 1412.6661

Swaters, R.A., van Albada, T.S., van der Hulst, J.M., Sancisi, R.: The Westerbork HI survey of spiral and irregular galaxies. I. HI imaging of late-type dwarf galaxies. Astron. Astrophys. **390**, 829–861 (2002). doi:10.1051/0004-6361:20011755, astro-ph/0204525

Tacconi, L.J., Neri, R., Genzel, R., Combes, F., Bolatto, A., Cooper, M.C., Wuyts, S., Bournaud, F., Burkert, A., Comerford, J., Cox, P., Davis, M., Förster Schreiber, N.M., García-Burillo, S., Gracia-Carpio, J., Lutz, D., Naab, T., Newman, S., Omont, A., Saintonge, A., Shapiro Griffin, K., Shapley, A., Sternberg, A., Weiner, B.: PHIBSS: molecular gas content and scaling relations in z ∼ 1-3 massive, main-sequence star-forming galaxies. Astrophys. J. **768**, 74 (2013). doi:10.1088/0004-637X/768/1/74, 1211.5743

Tremonti, C.A., Heckman, T.M., Kauffmann, G., Brinchmann, J., Charlot, S., White, S.D.M., Seibert, M., Peng, E.W., Schlegel, D.J., Uomoto, A., Fukugita, M., Brinkmann, J.: The origin of the mass-metallicity relation: insights from 53,000 star-forming galaxies in the Sloan Digital Sky Survey. Astrophys. J. **613**, 898–913 (2004). doi:10.1086/423264, astro-ph/0405537

Tripp, T.M., Giroux, M.L., Stocke, J.T., Tumlinson, J., Oegerle, W.R.: The ionization and metallicity of the intervening O VI absorber at z=0.1212 in the spectrum of H1821+643. Astrophys. J. **563**, 724–735 (2001). doi:10.1086/323965, astro-ph/0108371

Tumlinson, J.: Chemical evolution in hierarchical models of cosmic structure. I. Constraints on the early Stellar initial mass function. Astrophys. J. **641**, 1–20 (2006). doi:10.1086/500383, astro-ph/0507442

Tumlinson, J., Shull, J.M., Rachford, B.L., Browning, M.K., Snow, T.P., Fullerton, A.W., Jenkins, E.B., Savage, B.D., Crowther, P.A., Moos, H.W., Sembach, K.R., Sonneborn, G., York, D.G.: A far ultraviolet spectroscopic explorer survey of interstellar molecular hydrogen in the small and large magellanic clouds. Astrophys. J. **566**, 857–879 (2002). doi:10.1086/338112, astro-ph/0110262

Tumlinson, J., Prochaska, J.X., Chen, H.W., Dessauges-Zavadsky, M., Bloom, J.S.: Missing molecular hydrogen and the physical conditions of GRB host galaxies. Astrophys. J. **668**, 667–673 (2007). doi:10.1086/521294, astro-ph/0703666

Tumlinson, J., Thom, C., Werk, J.K., Prochaska, J.X., Tripp, T.M., Weinberg, D.H., Peeples, M.S., O'Meara, J.M., Oppenheimer, B.D., Meiring, J.D., Katz, N.S., Davé, R., Ford, A.B., Sembach, K.R.: The large, oxygen-rich halos of star-forming galaxies are a major reservoir of galactic metals. Science **334**, 948 (2011). doi:10.1126/science.1209840, 1111.3980

Tumlinson, J., Thom, C., Werk, J.K., Prochaska, J.X., Tripp, T.M., Katz, N., Davé, R., Oppenheimer, B.D., Meiring, J.D., Ford, A.B., O'Meara, J.M., Peeples, M.S., Sembach, K.R., Weinberg, D.H.: The COS-Halos survey: rationale, design, and a census of circumgalactic neutral hydrogen. Astrophys. J. **777**, 59 (2013). doi:10.1088/0004-637X/777/1/59, 1309.6317

van Zee, L., Salzer, J.J., Haynes, M.P., O'Donoghue, A.A., Balonek, T.J.: Spectroscopy of outlying H II regions in spiral galaxies: abundances and radial gradients. Astron. J. **116**, 2805–2833 (1998). doi:10.1086/300647, astro-ph/9808315

Verdes-Montenegro, L., Yun, M.S., Williams, B.A., Huchtmeier, W.K., Del Olmo, A., Perea, J.: Where is the neutral atomic gas in Hickson groups? Astron. Astrophys. **377**, 812–826 (2001). doi:10.1051/0004-6361:20011127, astro-ph/0108223

Verheijen, M., van Gorkom, J.H., Szomoru, A., Dwarakanath, K.S., Poggianti, B.M., Schiminovich, D.: WSRT ultradeep neutral hydrogen imaging of galaxy clusters at z ∼0.2: a pilot survey of Abell 963 and Abell 2192. Astrophys. J. Lett. **668**, L9–L13 (2007). doi:10.1086/522621, 0708.3853

Verheijen, M.A.W., Sancisi, R.: The Ursa Major cluster of galaxies. IV. HI synthesis observations. Astron. Astrophys. **370**, 765–867 (2001). doi:10.1051/0004-6361:20010090, astro-ph/0101404

Viegas, S.M.: Abundances at high redshift: ionization correction factors. Mon. Not. R. Astron. Soc. **276**, 268–272 (1995). doi:10.1093/mnras/276.1.268

Vladilo, G., Centurión, M., Bonifacio, P., Howk, J.C.: Ionization properties and elemental abundances in damped Lyα systems. Astrophys. J. **557**, 1007–1020 (2001). doi:10.1086/321650, astro-ph/0104298

Walter, F., Brinks, E., de Blok, W.J.G., Bigiel, F., Kennicutt, R.C. Jr., Thornley, M.D., Leroy, A.: THINGS: the H I nearby galaxy survey. AJ **136**, 2563–2647 (2008). doi:10.1088/0004-6256/136/6/2563, 0810.2125

Walter, F., Decarli, R., Sargent, M., Carilli, C., Dickinson, M., Riechers, D., Ellis, R., Stark, D., Weiner, B., Aravena, M., Bell, E., Bertoldi, F., Cox, P., Da Cunha, E., Daddi, E., Downes, D., Lentati, L., Maiolino, R., Menten, K.M., Neri, R., Rix, H.W., Weiss, A.: A molecular line scan in the hubble deep field north: constraints on the CO luminosity function and the cosmic H_2 density. Astrophys. J. **782**, 79 (2014). doi:10.1088/0004-637X/782/2/79, 1312.6365

Warren, S.J., Møller, P., Fall, S.M., Jakobsen, P.: NICMOS imaging search for high-redshift damped Lyα galaxies. Mon. Not. R. Astron. Soc. **326**, 759–773 (2001). doi:10.1046/j.1365-8711.2001.04629.x, astro-ph/0105032

Werk, J.K., Prochaska, J.X., Thom, C., Tumlinson, J., Tripp, T.M., O'Meara, J.M., Peeples, M.S.: The COS-Halos survey: an empirical description of metal-line absorption in the low-redshift circumgalactic medium. Astrophys. J. Suppl. Ser. **204**, 17 (2013). doi:10.1088/0067-0049/204/2/17, 1212.0558

Werk, J.K., Prochaska, J.X., Tumlinson, J., Peeples, M.S., Tripp, T.M., Fox, A.J., Lehner, N., Thom, C., O'Meara, J.M., Ford, A.B., Bordoloi, R., Katz, N., Tejos, N., Oppenheimer, B.D., Davé, R., Weinberg, D.H.: The COS-Halos survey: physical conditions and baryonic mass in the low-redshift circumgalactic medium. Astrophys. J. **792**, 8 (2014). doi:10.1088/0004-637X/792/1/8, 1403.0947

Westmeier, T., Brüns, C., Kerp, J.: Relics of structure formation: extra-planar gas and high-velocity clouds around the Andromeda Galaxy. Mon. Not. R. Astron. Soc. **390**, 1691–1709 (2008). doi:10.1111/j.1365-2966.2008.13858.x, 0808.3611

Wolfe, A.M., Chen, H.W.: Searching for low surface brightness galaxies in the hubble ultra deep field: implications for the star formation efficiency in neutral gas at $z \sim 3$. Astrophys. J. **652**, 981–993 (2006). doi:10.1086/507574, astro-ph/0608040

Wolfe, A.M., Turnshek, D.A., Smith, H.E., Cohen, R.D.: Damped Lyman-alpha absorption by disk galaxies with large redshifts. I - The Lick survey. Astrophys. J. Suppl. Ser. **61**, 249–304 (1986). doi:10.1086/191114

Wolfe, A.M., Lanzetta, K.M., Foltz, C.B., Chaffee, F.H.: The large bright QSO survey for damped LY alpha absorption systems. Astrophys. J. **454**, 698 (1995). doi:10.1086/176523

Wolfe, A.M., Gawiser, E., Prochaska, J.X.: Damped Ly α systems. Ann. Rev. Astron. Astrophys. **43**, 861–918 (2005). doi:10.1146/annurev.astro.42.053102.133950, astro-ph/0509481

Wolfire, M.G., Tielens, A.G.G.M., Hollenbach, D., Kaufman, M.J.: Chemical rates on small grains and PAHs: C^+ recombination and H_2 formation. Astrophys. J. **680**, 384–397 (2008). doi:10.1086/587688, 0803.0138

Wong, T., Blitz, L.: The relationship between gas content and star formation in molecule-rich spiral galaxies. Astrophys. J. **569**, 157–183 (2002). doi:10.1086/339287, astro-ph/0112204

Wright, S.A., Larkin, J.E., Law, D.R., Steidel, C.C., Shapley, A.E., Erb, D.K.: Dynamics of galactic disks and mergers at $z \sim 1.6$: spatially resolved spectroscopy with Keck laser guide star adaptive optics. Astrophys. J. **699**, 421–440 (2009). doi:10.1088/0004-637X/699/1/421, 0810.5599

Wuyts, E., Wisnioski, E., Fossati, M., Förster Schreiber, N.M., Genzel, R., Davies, R., Mendel, J.T., Naab, T., Röttgers, B., Wilman, D.J., Wuyts, S., Bandara, K., Beifiori, A., Belli, S., Bender, R., Brammer, G.B., Burkert, A., Chan, J., Galametz, A., Kulkarni, S.K., Lang, P., Lutz, D., Momcheva, I.G., Nelson, E.J., Rosario, D., Saglia, R.P., Seitz, S., Tacconi, L.J., Tadaki, K.I., Übler, H., van Dokkum, P.: The evolution of metallicity and metallicity gradients from $z = 2.7$ to 0.6 with KMOS^{3D}. Astrophys. J. **827**, 74 (2016). doi:10.3847/0004-637X/827/1/74, 1603.01139

Wyder, T.K., Martin, D.C., Barlow, T.A., Foster, K., Friedman, P.G., Morrissey, P., Neff, S.G., Neill, J.D., Schiminovich, D., Seibert, M., Bianchi, L., Donas, J., Heckman, T.M., Lee, Y.W., Madore, B.F., Milliard, B., Rich, R.M., Szalay, A.S., Yi, S.K.: The star formation law at low surface density. Astrophys. J. **696**, 1834–1853 (2009). doi:10.1088/0004-637X/696/2/1834, 0903.3015

York, D.G., Adelman, J., Anderson, J.E. Jr., Anderson, S.F., Annis, J., Bahcall, N.A., Bakken, J.A., Barkhouser, R., Bastian, S., Berman, E., Boroski, W.N., Bracker, S., Briegel, C., Briggs, J.W., Brinkmann, J., Brunner, R., Burles, S., Carey, L., Carr, M.A., Castander, F.J., Chen, B., Colestock, P.L., Connolly, A.J., Crocker, J.H., Csabai, I., Czarapata, P.C., Davis, J.E., Doi, M., Dombeck, T., Eisenstein, D., Ellman, N., Elms, B.R., Evans, M.L., Fan, X., Federwitz, G.R., Fiscelli, L., Friedman, S., Frieman, J.A., Fukugita, M., Gillespie, B., Gunn, J.E., Gurbani, V.K., de Haas, E., Haldeman, M., Harris, F.H., Hayes, J., Heckman, T.M., Hennessy, G.S., Hindsley, R.B., Holm, S., Holmgren, D.J., Huang, Ch., Hull, C., Husby, D., Ichikawa, S.I., Ichikawa, T., Ivezić, Ž., Kent, S., Kim, R.S.J., Kinney, E., Klaene, M., Kleinman, A.N., Kleinman, S., Knapp, G.R., Korienek, J., Kron, R.G., Kunszt, P.Z., Lamb, D.Q., Lee, B., Leger R.F., Limmongkol, S., Lindenmeyer, C., Long, D.C., Loomis, C., Loveday, J., Lucinio, R., Lupton, R.H., MacKinnon, B., Mannery, E.J., Mantsch, P.M., Margon, B., McGehee, P., McKay, T.A., Meiksin, A., Merelli, A., Monet, D.G., Munn, J.A., Narayanan, V.K., Nash, T., Neilsen, E., Neswold, R., Newberg, H.J., Nichol, R.C., Nicinski, T., Nonino, M., Okada, N., Okamura, S., Ostriker, J.P., Owen, R., Pauls, A.G., Peoples, J., Peterson, R.L., Petravick, D., Pier, J.R., Pope,

A., Pordes, R., Prosapio, A., Rechenmacher, R., Quinn, T.R., Richards, G.T., Richmond, M.W., Rivetta, C.H., Rockosi, C.M., Ruthmansdorfer, K., Sandford, D., Schlegel, D.J., Schneider, D.P., Sekiguchi, M., Sergey, G., Shimasaku, K., Siegmund, W.A., Smee, S., Smith, J.A., Snedden, S., Stone, R., Stoughton, C., Strauss, M.A., Stubbs, C., SubbaRao, M., Szalay, A.S., Szapudi, I., Szokoly, G.P., Thakar, A.R., Tremonti, C., Tucker, D.L., Uomoto, A., Vanden Berk, D., Vogeley, M.S., Waddell, P., Wang, S.I., Watanabe, M., Weinberg, D.H., Yanny, B., Yasuda, N., SDSS Collaboration: The Sloan Digital Sky Survey: technical summary. Astron. J. **120**, 1579–1587 (2000). doi:10.1086/301513, astro-ph/0006396

Yun, M.S., Ho, P.T.P., Lo, K.Y.: A high-resolution image of atomic hydrogen in the M81 group of galaxies. Nature **372**, 530–532 (1994). doi:10.1038/372530a0

Zahedy, F.S., Chen, H.W., Rauch, M., Wilson, M.L., Zabludoff, A.: Probing the cool interstellar and circumgalactic gas of three massive lensing galaxies at z = 0.4–0.7. Mon. Not. R. Astron. Soc. **458**, 2423–2442 (2016). doi:10.1093/mnras/stw484, 1510.04307

Zaritsky, D., Kennicutt, R.C. Jr., Huchra, J.P.: H II regions and the abundance properties of spiral galaxies. Astrophys. J. **420**, 87–109 (1994). doi:10.1086/173544

Zwaan, M.A.: Prochaska JX (2006) Where is the molecular hydrogen in damped Lyα absorbers? Astrophys. J. **643**, 675–679 doi:10.1086/503191, astro-ph/0601655

Zwaan, M.A., van der Hulst, J.M., Briggs, F.H., Verheijen, M.A.W., Ryan-Weber, E.V.: Reconciling the local galaxy population with damped Lyman α cross-sections and metal abundances. Mon. Not. R. Astron. Soc. **364**, 1467–1487 (2005). doi:10.1111/j.1365-2966.2005.09698.x, astro-ph/0510127